

# Investigation of the stellar content in the IRAS 05168+3634 star-forming region

N.M. Azatyan

Byurakan Astrophysical Observatory, 0213, Aragatsotn prov., Armenia  
e-mail: nayazatyan@bao.sci.am

Received ; accepted

## ABSTRACT

**Aims.** We report the investigation results of the structure and content of a molecular cloud surrounding the source IRAS 05168+3634 (also known as Mol 9).

**Methods.** We present a photometric analysis using the data of J, H, K UKIDSS, [3.6], [4.5]  $\mu$ m *Spitzer*-IRAC and 3.4, 4.6, 12, 22  $\mu$ m WISE databases. A multi-color criteria was used to identify the candidates of young stellar objects (YSOs) in the molecular cloud; in addition to IRAS 05168+3634, there are four IRAS sources embedded in the same molecular cloud. Color-magnitude diagrams and the K luminosity function (KLF) were used to determine the basic parameters of stellar objects (spectral classes, masses, ages). To study the YSOs with longer wavelength photometry the radiative transfer models were used.

**Results.** Based on color-color and color-magnitude diagrams, we identified a rich population of embedded YSO candidates with infrared excess (Class 0/I and Class II) and their characteristics in a quite large molecular cloud located in a region of 24 arcmin radius. The molecular cloud includes 240 candidates of YSOs within the radii of subregions around five IRAS sources. The local distribution of identified YSOs in the molecular cloud frequently shows elongation and subclustering. The observed young subregions and parental molecular cloud morphologies are similar, especially when only the youngest Class I/0 sources are considered. The color-magnitude diagrams of the subregions suggest a very young stellar population. We construct the KLF of the subregions except for the IRAS 05162+3639 region) and it shows unusually low values for  $\alpha$  slope: 0.12–0.21. According to the values of the slopes of the KLFs, the age of the subregions can be estimated at 0.1–3 Myr. The spectral energy distributions (SEDs) are constructed for 45 Class I and 75 Class II evolutionary stage YSOs and the received parameters of these YSOs are well correlated with the results obtained by other methods.

**Key words.** stars: pre-main sequence – stars: luminosity function – infrared: stars – radiative transfer – ISM: individual objects: IRAS 05168+3634

## 1. Introduction

Young embedded stellar clusters are important laboratories for understanding star formation process and early stellar evolution because they contain a statistically significant sample of stars formed from the same parental interstellar matter. The development of sensitive, large-format imaging arrays at near- and mid-infrared (NIR and MIR), submillimeter, and radio wavelengths has made it possible to obtain statistically significant and complete sampling of young embedded clusters within molecular clouds.

The widely accepted scenario of low- and intermediate-mass star formation is that they are formed by gravitational collapse, and the subsequent accretion of their parent molecular clouds and driving collimated outflows. However, the main mechanism leading to the formation of massive stars is debated as to whether it is disk accretion similar to that for lower mass stars (Yorke & Sonnhalter 2002). Unlike low-mass stars, the high-mass star evolution is a fast process that lasts for no more than about  $10^6$  yr including the main sequence. During their formation, massive stars usually stay within their birth sites in clustered environments (Guan et al. 2008a).

In this paper, we present a detailed study of a star-forming region in the vicinity of IRAS 05168+3634, which is also known as Mol 9 in the catalogue of Molinari et al. (1996). Within a 2 arcmin radius of IRAS 05168+3634, three objects have been

detected with magnitudes of the Midcourse Space Experiment (MSX) survey (Egan et al. 2003), one of which is associated with IRAS 05168+3634. Zhang et al. (2005) have discovered a molecular outflow in this region.

IRAS 05168+3634 is a luminous young stellar object (YSO) (longitude = 170.657, latitude = -00.27) with estimated  $L=24 \times 10^3 L_{\odot}$  (Varricatt et al. 2010); it is located in a high-mass star-forming region in the pre-UC HII phase (Wang et al. 2009). Compact HII regions and H<sub>2</sub>O maser are sites of ongoing high-mass star formation which have not completely disrupted the surrounding dense, molecular gas. Thus, we have an opportunity to examine the stellar population in its initial configuration, before the rapid dynamical evolution which may occur once the molecular gas is cleared by stellar winds and the expanding region (Lada et al. 1984). There have been various detections in the region: H<sub>2</sub>O maser emission (Zhang et al. 2005), NH<sub>3</sub> maser emission (Molinari et al. 1996), CS emission (Bronfman et al. 1996), a new detection of 44 GHz CH<sub>3</sub>OH methanol maser emission (Fontani et al. 2010), the SiO (J = 2–1) line (Harju et al. 1998), the main lines at 1665 MHz and 1667 MHz OH maser (Ruiz-Velasco et al. 2016), and four <sup>13</sup>CO cores (Guan et al. 2008b). No radio source has been associated with IRAS 05168+3634. Molinari et al. (1998) have detected 6 cm radio emission 102 arcsec away from IRAS 05168+3634.

The embedded stellar cluster in this region was detected in the NIR and MIR by various authors (Kumar et al. 2006; Faus-tini et al. 2009; Azatyan et al. 2016). In Azatyan et al. (2016) it was shown that this is a bimodal cluster with 1.5 arcmin radius from geometric center of the cluster that does not coincide with IRAS 05168+3634. One of the subgroups is concentrated around IRAS 05168+3634 and it should be noted that it does not contain a rich population compared to other concentrations.

The distance estimations of this region are different. A kinematic distance was estimated of 6.08 kpc (Molinari et al. 1996) based on systemic local standard of rest (LSR) velocity  $V_{LSR} = -15.5 \pm 1.9$  km/s. The trigonometric parallax of IRAS 05168+3634 with VERA is  $0.532 \pm 0.053$  mas, which corresponds to a distance of  $1.88^{+0.21}_{-0.17}$  kpc, placing the region in the Perseus arm rather than the Outer arm (Sakai et al. 2012). This large difference of estimated distances causes some significant differences in physical parameters for individual members.

In the present paper, we tabulate of the YSO candidates in this star-forming region and discuss their spatial distribution. The observational data used to make the subsequent analysis are discussed in Section 2. The results and discussion are given in Section 3, and Section 4 concludes with the results of this work.

## 2. Observational data

For our study we used the data covering a wide infrared (IR) range from NIR to far-infrared (FIR) wavelengths. The first is the archival NIR photometric data and images in the J, H, and K bands of the Galactic Plane Survey DR6 (GPS, Lucas et al. 2008) with a resolution of  $0.1''$ /px, which is one of the five surveys of the UKIRT Infrared Deep Sky Survey (UKIDSS). UKIDSS GPS is complete to approximately 18.05 K mag, and for individual objects provides a probability (in percent) of being a star, galaxy, and noise accessible in Vizier service.

Mid-IR wavelengths are ideal for studying disks because these wavelengths are well removed from the peak of the underlying stellar energy distribution, resulting in much greater excesses over the underlying stellar photosphere. Archival MIR observations of this region were obtained using the *Spitzer* Space Telescope under the Galactic Legacy Infrared Midplane Survey Extraordinaire 360 (GLIMPSE 360) program (Churchwell et al. 2009). GLIMPSE 360 observations were taken using the InfraRed Array Camera (IRAC, Fazio et al. 2004) in 3.6,  $4.5 \mu\text{m}$  bands with a resolution of  $0.6''$ /px. The point source photometric data in this star-forming region were downloaded from the NASA/IPAC Infrared Science Archive. We also used the Wide-field Infrared Survey Explorer (WISE, Wright et al. 2010) ( $3.4 \mu\text{m}$ ,  $4.6 \mu\text{m}$ ,  $12 \mu\text{m}$ , and  $22 \mu\text{m}$ ) and the MSX surveys ( $8.28 \mu\text{m}$ ,  $12.13 \mu\text{m}$ ,  $14.65 \mu\text{m}$ , and  $21.3 \mu\text{m}$ ) accessible in Vizier.

Since high-mass star formation happens deeply embedded, only observations at FIR and longer wavelengths can penetrate inside, and therefore provide essential information about such star-forming regions. This information may be provided by FIR wavelengths, in the range  $70\text{--}500 \mu\text{m}$ , obtained by using the Photodetector Array Camera and Spectrometer (PACS, Poglitsch et al. 2010) and the Spectral and Photometric Imaging Receiver (SPIRE, Griffin et al. 2010) on the 3.5 m *Herschel* Space Observatory (Pilbratt et al. 2010). For our analyses, we used PACS 70,  $160 \mu\text{m}$  and SPIRE 250, 350, and  $500 \mu\text{m}$  photometric data and images with resolutions varying from  $\sim 5.5''$  to  $36''$ . The point and extended source photometry were downloaded from the NASA/IPAC Infrared Science Archive. *Herschel* PACS data have better resolution with respect to the IRAS mission data; for

this reason we used the data from the *Herschel* PACS 70 and  $160 \mu\text{m}$  catalogs instead of IRAS 60 and  $100 \mu\text{m}$  data.

## 3. Results and discussion

### 3.1. Structure of the molecular cloud

The IRAS 05168+3634 star-forming region has a more complicated structure in the FIR wavelengths than in the NIR and MIR. The complex structure of the region is clearly visible especially in the images of the *Herschel* PACS  $160 \mu\text{m}$  and SPIRE 250, 350,  $500 \mu\text{m}$  bands. Figure 1 shows the region in different wavelengths from NIR to FIR. Moving toward longer wavelengths in the *Herschel* PACS  $160 \mu\text{m}$  and the SPIRE 250, 350,  $500 \mu\text{m}$  bands images, the cloud filaments surrounding IRAS 05168+3634 become more visible and it is obvious that the IRAS 05168+3634 star-forming region is not limited in 1.5 arcmin radius from geometric center (Azatyan et al. 2016) but is more extended and is located within a 24 arcmin radius molecular cloud where the center of the molecular cloud is the conditionally selected source IRAS 05168+3634. Studying the common star-forming region in the molecular cloud, it turns out that apart from IRAS 05168+3634, there are four IRAS sources (IRAS 05184+3635, IRAS 05177+3636, IRAS 05162+3639, and IRAS 05156+3643) embedded in the same molecular cloud. On the MIR  $[4.5] \mu\text{m}$  band image can be clearly seen that these IRAS objects, like IRAS 05168+3634, have a concentration of sources around them. There is very little information about these IRAS sources. IRAS 05184+3635 and IRAS 05177+3636 are associated with dark clouds DOBASHI 4334 and 4326, respectively (Dobashi 2011). In Casoli et al. (1986) the distances of IRAS 05184+3635 and IRAS 05177+3636 were assessed based on the  $^{13}\text{CO}$  velocities:  $-17$  km/s and  $-15$  km/s, respectively, as a result of which both IRAS 05184+3635 and IRAS 05177+3636 were evaluated at the same 1.4 kpc distance. The latter value coincides with the distance of IRAS 05168+3634 based on trigonometric parallax. This also indicates that these IRAS sources are most likely to be found in the same molecular cloud. On the other hand, Wouterloot & Brand (1989) estimated the distance of IRAS 05184+3635 based on the CO ( $J = 1 - 0$ ) line parameters, taking into account the same  $-17$  km/s velocity value, at a distance of 9.4 kpc. It should be noted that it is hard to say which of the estimated distances is correct. There are two objects near IRAS 05177+3636 detected at submillimeter wavelengths (Di Francesco et al. 2008). IRAS 05162+3639 is associated with the  $\text{H}_2\text{O}$  maser (Sunada et al. 2007). A high proper-motion star has been detected in the LSPM-NORTH catalog 0.35 arcmin from the IRAS 05156+3643 (Lépine & Shara 2005) probably compatible with IRAS 05156+3643 within the error bars.

We have constructed a map of the distribution of stellar surface density within a  $48' \times 48'$  region to investigate the structure of each concentration in the molecular cloud, using photometric data of the *Herschel* PACS Point Source Catalog:  $160 \mu\text{m}$  and Extended Source List (red band). The density was determined simply by dividing the number of stellar objects in a  $200'' \times 200''$  area with a step size of  $100''$ . Figure 2 shows the map of the distribution of stellar surface density based on *Herschel* PACS  $160 \mu\text{m}$  photometry.

In the case of the homogeneous distribution of stars in the field, it is known that the number of stars is comparable to the surface area occupied by those stars. We wanted to determine how much the distribution of stars in this field differs from the homogeneous distribution. Table 1 shows the surface area of all

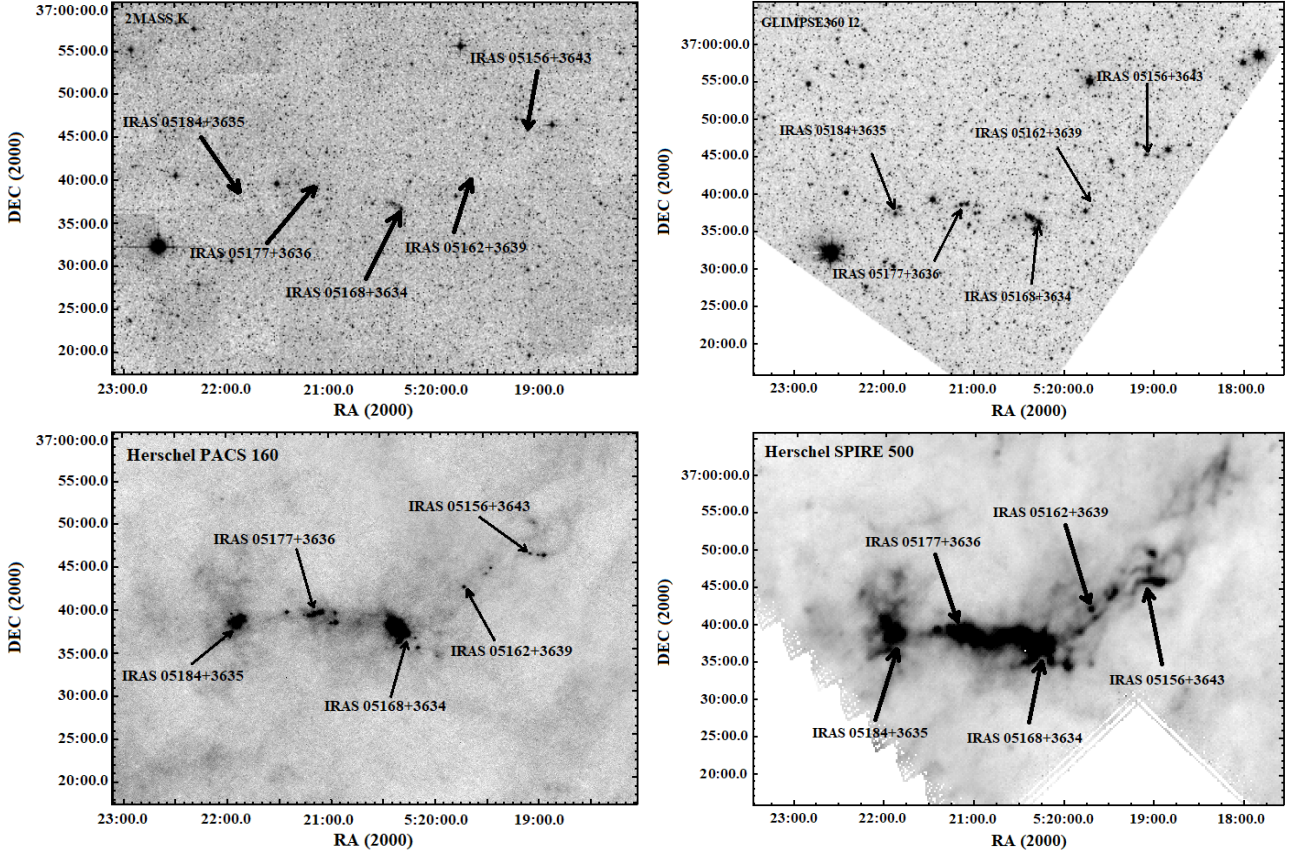


**Fig. 1.** Investigated region in different wavelengths. Top left and right panels show the region in NIR (2MASS K band) and MIR (GLIMPSE 360 I2 band) wavelengths, respectively. Bottom left and right panels show the region in FIR wavelengths: *Herschel*: PACS 160 and SPIRE 500, respectively. The position of five IRAS sources are indicated by arrows.

subregions according to the isodences in Col. 2 and the number of stars on those surface areas in Col. 3. The labels  $S_{TR}$  and  $S_{Total}$  are the total surface area of five subregions and the surface area within a 24 arcmin radius (IRAS 05168+3634 is considered the center), respectively. The ratios of  $S_{TR}/S_{Total}=0.02$  and  $N_{TR}/N_{Total}=0.7$  indicate what fraction of the surface area within a 24 arcmin radius is the total surface area of the subregions and how much of the objects in the whole field are on the total surface area of the subregion, respectively. From these values, it is possible to estimate the difference between the distribution of stars in our field and the homogeneous distribution. As a result, the distribution of stars in our field is 35 times different from the homogeneous distribution, which is a fairly high value. On the other hand, the distribution of sources in the field repeats the shape of the molecular cloud seen in FIR wavelengths, which suggests that the distribution of these subregions is not accidental, that is, they are connected to each other and belong to the same molecular cloud. From this, we can conclude with high probability that all five IRAS star-forming regions are at the same distance. Since only the IRAS 05168+3634 star-forming region has estimated distances (see Section 1), we can say that IRAS 05184+3635, IRAS 05177+3636, IRAS 05162+3639, and IRAS 05156+3643 are also located at a distance of 6.08 kpc (kinematic estimation) or  $1.88^{+0.21}_{-0.17}$  kpc (based on the trigonometric parallax). These distance estimations are used in future calculations in this paper.

**Table 1.** Sizes and contents of the subregions

Name	Surface area (arcmin <sup>2</sup> )	Objects
(1)	(2)	(3)
IRAS 05184+3635	5.245	6
IRAS 05177+3636	10.072	7
IRAS 05168+3634	11.14	7
IRAS 05162+3639	5.384	6
IRAS 05156+3643	10.068	6
	$S_{TR} = 41.909$	$N_{TR} = 32$
	$S_{Total} = 1808.64$	$N_{Total} = 43$

**Notes.** (1) Name of the subregions, (2) Approximate surface area of each subregion based on *Herschel* PACS 160  $\mu$ m catalog data, (3) Number of objects in each subregion based on *Herschel* PACS 160  $\mu$ m catalog data.

### 3.2. Selection of objects

For the selection of objects in the molecular cloud, we used the data of NIR, MIR, and FIR catalogs (see Section 2) within a radius of 24 arcmin concerning the conditionally selected IRAS 05168+3634. We chose GPS UKIDSS-DR6 as the main catalog, and the other catalogs were cross-matched with it. As was mentioned in Section 2, the GPS UKIDSS-DR6 catalog for individual objects provides a probability (in percent) of being



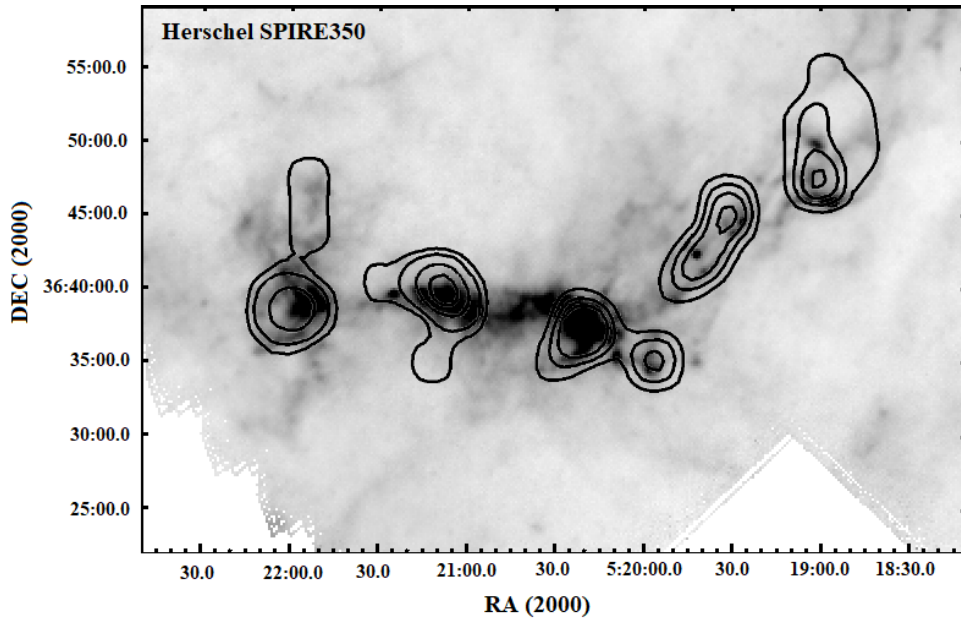


**Fig. 2.** Stellar surface density distribution based on *Herschel* PACS 160  $\mu\text{m}$  photometry. Stellar surface density distribution map is overplotted on *Herschel* SPIRE 350  $\mu\text{m}$  image. The surface density of the last isodensities exceeds the average value of the field surface density on  $1\sigma$

**Table 2.** Properties of used catalogs

Catalog name	Positional accuracy (arcsec)	$3\sigma$ of combined error (arcsec)	Reference
(1)	(2)	(3)	(4)
GPS UKIDSS-DR6	0.3	–	1
GLIMPSE 360	0.3	1.2	2
ALLWISE	1	3	3
MSX	3.3	10	4
IRAS	16	48	5
PACS:Extended source	2.4	7.2	6
PACS: 70 $\mu\text{m}$	1.5	5	7
PACS: 160 $\mu\text{m}$	1.7	5.2	8
SPIRE:250,350,500 $\mu\text{m}$	1.7	5.2	9

**References.** 1. Lucas et al. (2008); 2. Churchwell et al. (2009); 3. Wright et al. (2010); 4. Egan et al. (2003); 5. Neugebauer et al. (1984); 6. Maddox et al. (2017); 7. Poglitsch et al. (2010); 8. Poglitsch et al. (2010); 9. Griffin et al. (2010).

**Notes.** (1) Name of catalog used, (2) Positional accuracy of each catalog, (3)  $3\sigma$  of combined error of cross-matched catalogs, (4) Source of data used.

a star, galaxy, and noise; therefore, we selected objects with a probability of being noise  $< 50\%$ , and taking into account the completeness limit of UKIDSS survey in K band, the objects that have a measured magnitude of  $K \geq 18.02$  were removed from the list. This yielded approximately 48000 objects. The MIR and FIR photometric catalogs were cross-matched with the GPS UKIDSS-DR6 catalog within  $3\sigma$  of combined error matching radius (Col. 3 in Table 2). Matching radii are evaluated taking into account the positional accuracy of each catalog (Col. 2 in Table 2). However, several catalogs provide photometric measurements for extended sources, for which positional errors are larger than values provided in catalogs. These catalogs are the *Herschel* PACS Point Source Catalog: Extended Source List and the *Herschel* SPIRE Point Source Catalog: 250,350,500  $\mu\text{m}$ ; therefore, the cross-match was done by eye for these catalogs and then a combined photometric catalog was obtained. In the next sections, the set of steps that we used to identify the YSOs.

### 3.3. Color-color diagrams

According to the star formation theory, the IR excess of young stars is caused by a circumstellar disk and gas-dust envelope, which are known as two of the main characteristics of YSOs (Lada & Lada 2003; Hartmann 2009). Therefore, it is possible to carry out the selection of YSOs in the region as they contain the IR excess in the NIR and/or MIR ranges.

One of the most powerful tools for identifying YSO candidates via reddening and excess is their location on color-color diagrams. The choice of colors depends on the available data. We have constructed four color-color diagrams. The investigated region is quite large and there is a high probability of selecting objects that do not belong to the molecular cloud as a result of photometric measurement errors; therefore, we chose as YSOs those stars that are classified as objects with IR excess in at least two color-color diagrams to minimize the likelihood of choosing incorrectly.

The first IR excess object identification was carried out with (J-H) versus (H-K) color-color diagram. Figure 3 (top left panel) shows the (J-H) versus (H-K) color-color diagram where the solid and dashed curves represent the locus of the intrinsic colors of dwarf and giant stars, taken from Bessell & Brett (1988) after being converted to the CIT system using the relations given by Carpenter (2001). The parallel solid lines drawn from the base and tip of the dwarf and giant loci, are the interstellar reddening vectors (Rieke & Lebofsky 1985). The locus of unreddened classical T Tauri stars (CTTSs) is taken from Meyer et al. (1997). The region bounded by the dashed lines where the pre-main sequence (PMS) stars with intermediate mass, i.e., Herbig Ae/Be stars are usually found (Hernández et al. 2005). The objects with different evolutionary stages have certain places in this diagram (Lada & Adams 1992): Classical Be stars, objects located to the left and objects located to the right of reddening vectors. Classical Be stars have  $J-K < 0.6$  and  $H-K < 0.3$  color indexes, and we removed them from the list. There is no real physical explanation for those objects which are located to the left of reddening vectors, so we also removed these objects. However, it is possible that among Classical Be stars and objects located to the left

of reddening vectors that there will be objects that belong to a molecular cloud. For further study, we chose objects located to the right of reddening vectors and the deviation of YSOs from the main sequence (MS) on this diagram can have two causes: the presence of IR excess and interstellar absorption, which also leads to the reddening of an object. In the latter case, the deviation from MS will be directed along reddening vectors. We have selected as YSOs those stars that have a considerable, accurately expressed IR excess.

The reddening of classified YSOs cannot be caused only by interstellar absorption and, at least partially, IR excess is created by presence of a circumstellar disk and an envelope. Therefore, the objects that are located to the right of reddening vectors in the (J-H) versus (H-K) diagram can be considered YSO candidates. Among the selected YSOs and objects within the reddening band of the MS and giant, we classified as Class I evolutionary stage objects those which have  $(J-K) > 3$  mag color index (Lada & Adams 1992) and located in the top right in the (J-H) versus (H-K) diagram. Other objects in the reddening band are generally considered to be either field stars or Class III objects with comparably small NIR excess, and making the right selection among them is very difficult, so we added to our list those objects classified as YSOs in at least two other color-color diagrams.

Not all objects in the main sample were detected in J, H, K bands simultaneously; therefore, we used the data of the GLIMPSE 360 catalog to construct color-color diagram combining NIR and MIR photometry in order to identify sources with IR excesses and to compile a more complete excess/disk census for the region. Since the  $4.5\mu\text{m}$  band is the most sensitive band to YSOs of the four IRAC bands (Gutermuth et al. 2006), we used the K-[3.6] versus [3.6]-[4.5] color-color diagram. Figure 3 (top right panel) shows the K-[3.6] versus [3.6]-[4.5] color-color diagram, where the diagonal lines outline the region of location of YSOs with both Class I and Class II evolutionary stages. The dereddened colors are separated into Class I and II domains by the dashed line. Arrow shows the extinction vector (Flaherty et al. 2007). All the lines in the K-[3.6] versus [3.6]-[4.5] diagram are taken from Allen et al. (2007). Both the (J-H) versus (H-K) and the K-[3.6] versus [3.6]-[4.5] color-color diagrams are widely used for the separation of YSOs with different evolutionary classes (Meyer et al. 1997; Gutermuth et al. 2006; Allen et al. 2007).

We also constructed two other color-color diagrams using the list of objects with good WISE detections, i.e., those possessing photometric uncertainty  $< 0.2$  mag in WISE bands. Figure 3 (lower left panel) shows the [3.4]-[4.6] versus [4.6]-[12] color-color diagram. As was mentioned for the previous color-color diagrams, the objects with different evolutionary stages are located in certain places in this diagram too (Koenig et al. 2012), i.e., Class I YSOs are the reddest objects, and are selected if their colors match  $[3.4]-[4.6] > 1.0$  and  $[4.6]-[12] > 2.0$ . Class II YSOs are slightly less red objects and are selected with colors  $[3.4]-[4.6]-\sigma([3.4]-[4.6]) > 0.25$  and  $[4.6]-[12]-\sigma([4.6]-[12]) > 1.0$ , where  $\sigma(\dots)$  indicates a combined photometric error, added in quadrature.

We can check the accuracy of previous classification of stars that possess photometric errors  $< 0.2$  mag in WISE band 4. Previously classified Class I sources were re-classified as Class II if  $[4.6]-[22] < 4.0$  and Class II stars have been placed back in the unclassified pool if  $[3.4]-[12] < -1.7 \times ([12]-[22]) + 4.3$  (Koenig et al. 2012). However, there are no incorrect selections in the pre-classified objects with 1, 2, 3 bands and it confirms the results obtained in the [3.4]-[4.6] versus [4.6]-[12] color-color diagram (Figure 3, lower right panel).

In total, we selected 1224 YSOs within a 24 arcmin radius, and they are indicated with filled circles. IRAS and MSX sources are indicated by triangles and squares, respectively, and they are labeled in the diagrams. Unfortunately, with this kind of selection of YSOs we cannot find the exact number of YSOs. T Tauri objects with comparably small amounts of NIR excesses may be located in the reddening band, and therefore are excluded from the selection. On the other hand, there can be fore-/background objects among the selected YSOs.

Figure 4 shows the distribution of classified YSOs in the field. Class I and Class II objects are indicated by filled circles and crosses, respectively. It can be clearly seen from the image that Class II objects are distributed more homogeneously on the field than Class I objects, which are located in certain areas and show clear concentrations. This confirms the assumption that, unlike the Class II objects, Class I objects did not have enough time to leave their birthplaces after formation. There are several Class I objects in the field that are far from the main concentrations, and because the distribution of Class I objects is closer to the initial distribution it can be argued that the Class I objects either have some measurement errors in magnitudes or that they do not belong to the molecular cloud. Since the distribution of stars and clearly visible concentrations repeat the shape of the molecular cloud, the probability of superposition is very small because in that case there would be other similar concentrations in the field, which are not detected outside the molecular cloud filaments.

Since the region is quite large, the probability of being fore-/background objects within the selected Class II objects is very high, and in the case of Class I objects that possibility is small as they are not detected outside the molecular cloud filaments. In order to minimize the number of incorrect Class II objects, further investigations will only be performed on concentration areas. For that purpose, we have constructed map of the distribution of stellar surface density within a  $48' \times 48'$  region to investigate the structure and size of each concentration in the molecular cloud, using the coordinates of selected YSOs. The contours of the distribution of stellar surface density is overplotted on Figure 4 and four subregions are clearly seen, each one surrounding one IRAS source. We refined the radius of each subregion relative to their geometric centers based on the density distribution of selected YSOs. The stellar density was determined for each ring of width  $0.1'$  by dividing the number of stars by the surface area. The radius of the subregions was considered the value from which according to Poisson statistics the fluctuations of the stellar density in the rings become random. Table 3 presents the coordinates of IRAS sources in Cols. 2 and 3, the coordinates of geometric centers are in Cols. 4 and 5, and the radii based on stellar density distribution are in the last column. There is no evidence of a real concentration only around IRAS 05162+3639. On the other hand, two objects from the GPS UKIDSS-DR6 catalog were identified with IRAS 05162+3639 as a result of a cross-match, i.e., IRAS 05162+3639 is probably a binary object and three more Class I objects are located very close to it, but they do not show any real concentration. Therefore, the 0.25 arcmin value of radius given in Table 3 is conditional and includes these three Class I objects and the binary associated with IRAS 05162+3639. As was already mentioned above, the objects within the determined radii will be explored in greater detail, so further studies will be conducted for the 240 YSOs of the 1224 selected from color-color diagrams; this total number of objects falls within the already-defined radii of five subregions. However, with this kind of choice, we lose a large number of objects that are actually located in the molec-

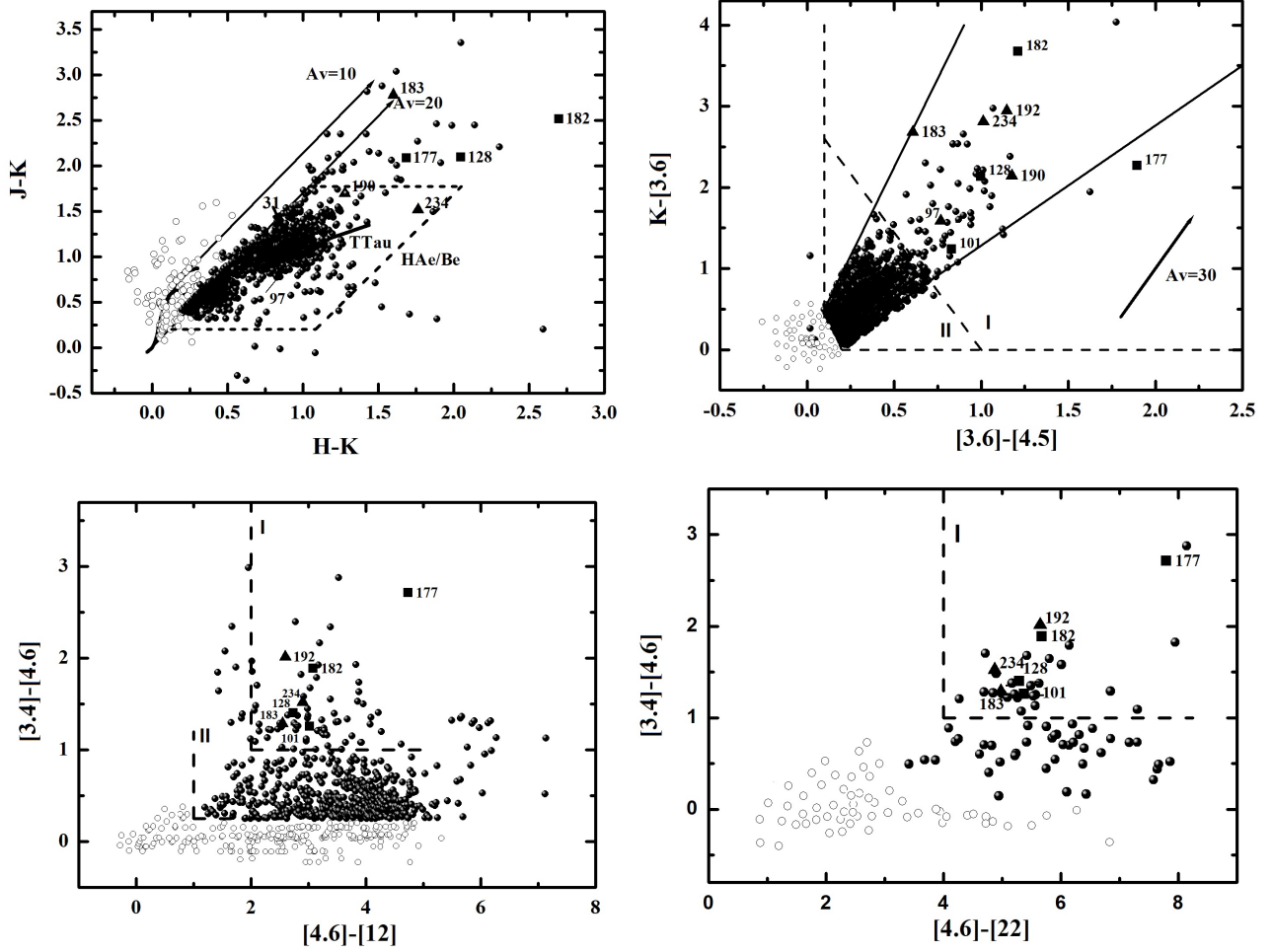


**Fig. 3.** Color-color diagrams of the region. In the top left panel is shown the (J-H) vs. (H-K) diagram. The dwarf and giant loci (solid and dashed curves, respectively) are from [Bessell & Brett \(1988\)](#) and were converted to the CIT system ([Carpenter 2001](#)). The parallel lines represent the interstellar reddening vectors ([Rieke & Lebofsky 1985](#)). The locus of unreddened classical T Tauri stars is from [Meyer et al. \(1997\)](#), and the region bounded by dashed lines is the Herbig Ae/Be stars location ([Hernández et al. 2005](#)). In the top right panel the K-[3.6] vs. [3.6]-[4.5] diagram is presented. In this diagram Class I and II domains are separated by the dashed line. The arrow shows the extinction vector ([Flaherty et al. 2007](#)). All the lines in the K-[3.6] vs. [3.6]-[4.5] diagram are from [Allen et al. \(2007\)](#). In bottom left and right panels are shown the [3.4]-[4.6] vs. [4.6]-[12] and [3.4]-[4.6] vs. [4.6]-[22] diagrams. The filled circles are selected YSOs and open circles are unclassified ones. Not all unclassified objects are presented in these diagrams. IRAS and MSX sources are indicated by triangles and squares, respectively, and they are labeled (see Tables 5 and 6).

ular cloud filaments but are left out of the determined radius of subregions. Otherwise, we would increase the number of non-members. Therefore, in this case, it would be possible to insist that the objects belonging to the molecular cloud were chosen as accurately as possible and that each subregion represents a separate star-forming region. Table 5 shows the catalog of 240 selected YSOs with NIR and MIR photometry, while Table 6 presents the fluxes for those YSOs which have FIR photometry. In the *Herschel* SPIRE 250, 350, 500  $\mu$ m catalogs, the photometry of objects was determined by four methods: Timeline Fitter value (TML), Daophot, Sussextractor, and Timeline Fitter 2 (TM2). For the slightly extended sources that were accepted in the *Herschel* SPIRE 250, 350, 500  $\mu$ m catalog, the TM2 value provides the best guess for an extended flux ([Griffin et al. 2010](#)). All selected YSOs in subregions that have measured fluxes at the 250, 350, 500  $\mu$ m wavelengths are classified as extended sources in the *Herschel* SPIRE 250, 350, 500  $\mu$ m catalogs. Taking into account the above, only TM2 photometry is presented in Table 6.

**Table 3.** Geometric centers of subregions

IRAS	$\alpha(2000)$ (hh mm ss)	$\delta(2000)$ (dd mm ss)	$\alpha(2000)$ (hh mm ss)	$\delta(2000)$ (dd mm ss)	Radius (arcmin)
(1)	(2)	(3)	(4)	(5)	(6)
05184+3635	05 21 53.2	+36 38 20.4	05 21 52.6	+36 39 07.1	2.5
05177+3636	05 21 09.4	+36 39 37.1	05 21 02.8	+36 38 28.5	3.5
05168+3634	05 20 16.4	+36 37 18.7	05 20 22.3	+36 37 33.9	3
05162+3639	05 19 38.4	+36 42 25.0	05 19 38.4	+36 42 25.0	0.25
05156+3643	05 19 03.6	+36 46 15.7	05 19 04.0	+36 48 02.0	2.8

**Notes.** (1)-Name of subregions, (2),(3)-The coordinates of IRAS sources, (4),(5)-The coordinates of geometric centers, (6)-The radius of each subregion according to YSOs surface density distribution in the molecular cloud

### 3.4. Color-magnitude diagrams

The color-magnitude diagram is a useful tool for studying the nature of the stellar population within star-forming regions and for estimating its spectral types. The distribution of the 240 iden-



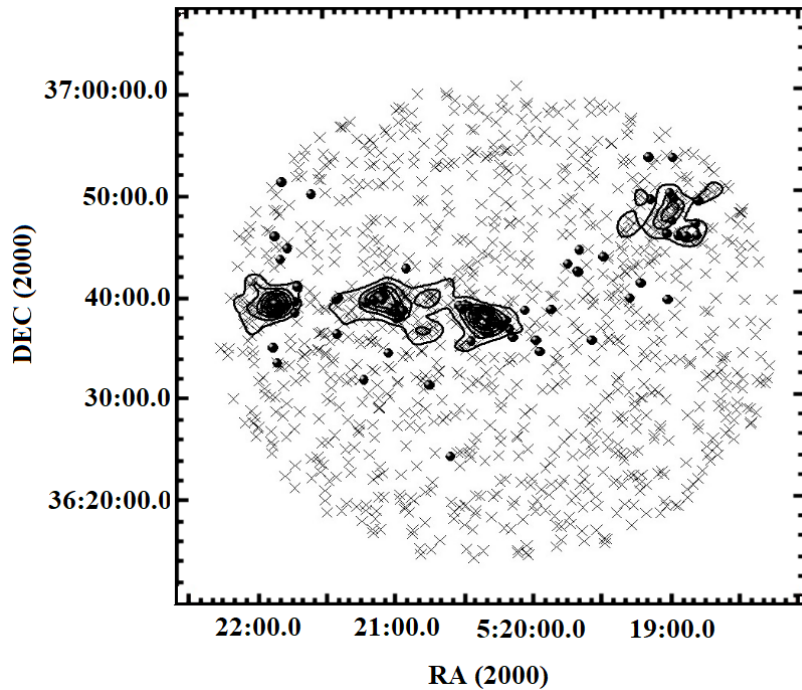


**Fig. 4.** Stellar surface density distribution based on color-color diagrams. Class I and Class II evolutionary stage objects are indicated by filled circles and crosses, respectively.

tified YSOs in the K versus J-K color-magnitude diagrams are shown in Figure 5 with different symbols for each subregion. We use the K versus J-K diagram because with this combination we get the maximum contrast between the IR excess produced by the presence of the disk, which affects mostly K, and the interstellar extinction, which has a greater effect on J. In Figure 5 the zero age main sequence (ZAMS, thick solid curve) and PMS isochrones for ages 0.1, 0.5, and 5 Myr (thin solid curves) are taken from Siess et al. (2000). We used the conversion table of Kenyon et al. (1994). The J and K photometry of the selected YSOs are corrected for two different distances: 6.1 and 1.88 kpc because, as mentioned above, all subregions with high probability are located at the same distance (see Section 3.1).

According to the COBE/DIRBE and IRAS/ISSA maps (Schlegel et al. 1998), we have estimated the interstellar extinction ( $A_v$ ) values toward five IRAS sources provided in Table 4. There is data of observations of  $^{13}\text{CO}$  cores, providing  $N_{H_2} = 4.5 \times 10^{21} \text{ cm}^{-2}$  column density (Guan et al. 2008b), only in the IRAS 05168+3634 star-forming region and using the conversion factor between column density and interstellar extinction  $N_{H_2} = 9.4 \times 10^{20} \text{ cm}^{-2}$  ( $A_v$ , mag) (Bohlin et al. 1978) have we received a value of  $A_v=4.8$  mag for interstellar extinction. The average of both interstellar extinction values ( $A_v=4.5$  mag) for the IRAS 05168+3634 star-forming region is used to correct the J and K magnitudes. Correction of the J and K magnitudes for the other four regions was done with the interstellar extinction estimated according to the COBE/DIRBE and IRAS/ISSA maps.

In general, the selected YSOs (according to the color-color diagrams) are distributed to the right of 0.1 Myr isochrones especially in the case of 6.1 kpc distance, and this distribution confirms that they are YSOs. The YSOs associated with IRAS and MSX sources are located within the range of the largest IR excess sources in both color-magnitude diagrams. Only a few identified as YSOs objects in the color-color diagrams are located to the left (open circles) of ZAMS, which means non-membership,

i.e., they are probably fore-/background objects. At different distances, the numbers of non-members are different, but it must be taken into account that the J and K magnitude corrections we made for objects belonging to an individual subregion using interstellar extinction values estimated toward IRAS sources only, which means those values would be different from the interstellar extinction values toward each object, and as a result some objects fall left of ZAMS. Thus, those objects were not removed from the list of YSOs (Table 5), but are shown as open circles in both color-magnitude diagrams. The results of the selection with the color-color and color-magnitude diagrams are presented in the Table 4 separately for each subregion depending on distance.

According to the results of color-color and color-magnitude diagrams, within the selected radius of each subregion the youngest is the IRAS 05168+3634 star-forming region since Class I objects represent a fairly large percentage. The next youngest subregion by Class I objects is IRAS 05177+3636, and it should be noted, even though there is no real concentration around IRAS 05162+3639, that only the Class I objects are inside the conditional selected radius. Finally, the subregions around IRAS 05184+3635 and IRAS 05156+3643 in the outer part of the molecular cloud are the oldest. However, it must be kept in mind that Class II objects have had enough time after formation and have left their birthplaces, so perhaps most of them are beyond the determined dimensions of subregions. Table 4 shows the percentage of Class I objects in each subregion.

The distribution of the YSOs on the K versus J-K color-magnitude diagram can be used to estimate their approximate age and mass based on the evolutionary models for objects with ages older than 1 Myr (Preibisch 2012). It is evident from Figure 5 that the YSOs in the molecular cloud in general are distributed to the right of 1 Myr isochrone, where the estimation of age and mass of those YSOs will be incorrect.

However, the color-magnitude diagrams show a certain distribution of mass in each subregion. Let us try to estimate the

mass limit for each subregion. Since NIR color excess, displayed in the color-color diagrams (Figure 3), is usually caused by the presence of disks around young stars, then by incorporating theoretical accreting disk models, the excess effect on the K versus J-K diagram can be accurately represented by vectors of approximately constant slope for disks around Class II T Tauri stars. The components of the vector are (1.01, -1.105) and (1.676, 1.1613) in magnitude units (López-Chico & Salas 2007). More massive YSOs are usually much more embedded than T Tauri stars, and that correction is unlikely to apply to such objects. However, the presence of a spherical envelope around the disk should cause a greater decrease in J-K for the same variation in K, than in the case of a “naked” disk (Cesaroni et al. 2015). Therefore, the López-Chico & Salas (2007) correction can be used to obtain a lower and an upper limit to the mass of each subregion for two different distances. Table 4 shows the results of mass completeness limit determination. Objects located in the IRAS 05184+3635, IRAS 5168+3634, and IRAS 05156+3643 star-forming regions are explicitly targeted at specific mass ranges for two distances, and for objects in the IRAS 05177+3636 star-forming region there is no similar dependency. It can be seen in color-magnitude diagrams and from estimated values of mass completeness limit shown in Table 4 Cols. 10 and 11. For the total content of four real subregions based on excess vector analysis, the following result is derived. At a distance of 1.88 kpc, approximately 80 % of the total content of the subregions have  $< 1$  solar mass, and the remaining  $\sim 20$  % objects have 1–3 solar masses. Only two objects have  $> 7$  solar masses that are clearly distinguished from the rest of the objects in the color-magnitude diagrams. At a distance of 6.1 kpc, approximately 20 % of the total content of the subregions have  $< 1$  solar mass, about 70 % objects have 1–3 solar masses, and the mass was estimated in the range 3–7 solar masses in only 7 % of the cases. There are only five objects with mass  $> 7$  solar masses.

The luminosity function in the K-band (KLF) is frequently used in studies of young clusters and star-forming regions as a diagnostic tool of the initial mass function (IMF) and the star formation history of their stellar populations (Zinnecker et al. 1993; Lada & Lada 1995; Jose et al. 2012). Thus, the observed KLF is a result of the IMF, the PMS evolution, and the star-forming history. Due to the uncertainty in the selected YSO ages (see Figure 5), it is impossible to derive an individual mass for each source and therefore the mass-luminosity relation cannot be constructed in order to get the IMF. Nevertheless, it is possible to construct the KLF to constrain the age of the embedded stellar population in each star-forming region independently. As pointed out by Lada et al. (1996), the age of a subregion can be estimated by comparing its KLF to the observed KLFs of other young clusters, i.e., the KLF slope could be an age indicator of young clusters. The KLF can be defined as  $dN(K)/dK \propto 10^{\alpha K}$ , where  $\alpha$  is the slope of the power law and  $N(K)$  is the number of stars brighter than  $K$  mag. The KLF slope is estimated by fitting the number of YSOs in 1 mag bins using a linear least-squares fitting routine. Since the slope is not affected by the intracluster extinction as long as the extinction is independent of the stellar mass (Megeath et al. 1996), we can use all the sources in the sample to define the slope without the complication of extinction correction. Therefore, Figure 6 shows the observed KLFs of YSOs detected in four subregions separately. In the case of the IRAS 05162+3639 subregion, there are not enough YSOs to construct the KLF and so it is impossible to estimate the value of the  $\alpha$  slope. The KLFs corresponding fitted slopes are provided in Table 4, which are lower than the typical values reported for young embedded clusters ( $\alpha \sim 0.4$ ; e.g., Lada et al. 1991; Lada & Lada 2003; Baug et al. 2015) and within the errors, the KLFs for all four subregions seem to match each other. For clusters up to 10 Myr old, the KLF slope gets steeper as the cluster gets older (Ali & Depoy 1995; Lada & Lada 1995). There are many studies on the



**Table 4.** Characteristics of subregions

IRAS	CCD		CMD-1.88 kpc		CMD-6.1 kpc		Class I	$A_V$ (mag)	Mass limit $M_{sun}$		$\alpha$ slope
	Mem.	Class I (%)	Mem.	Class I (%)	Mem.	Class I (%)			1.88kpc	6.1kpc	
(1)	(2)	(3)	(4)	(5)	(6)	(7)	(8)	(9)	(10)	(11)	(12)
05184+3635	52	21	48	23	52	21	11	1.4	0.3-1.5	0.8-5	$0.12 \pm 0.04$
05177+3636	79	28	65	34	79	28	22	1.34	0.2-2.2	0.7- >7	$0.2 \pm 0.02$
05168+3634	57	43	45	54	56	45	24	4.3 (4.5)	0.5-2.5	0.9- >7	$0.21 \pm 0.05$
05162+3639	5	—	5	—	5	—	5	1.23	—	—	—
05156+3643	47	20	40	23	47	20	9	1.03	0.2-1.6	0.6-3	$0.15 \pm 0.04$

**Notes.** (1) Name of subregions, (2) and (3) Number of YSOs and the fraction of Class I objects (in percent) according to the color-color diagrams, (4)–(7) Number of YSOs and the fraction of Class I objects (in percent) according to the color-magnitude diagrams in different distances, (8) Number of Class I evolutionary stage objects, (9) Interstellar extinction according to the COBE/DIRBE and IRAS/ISSA maps, (10)–(11) Mass completeness limits of each subregion in two distances, (12) The  $\alpha$  slope of KLF of each subregion

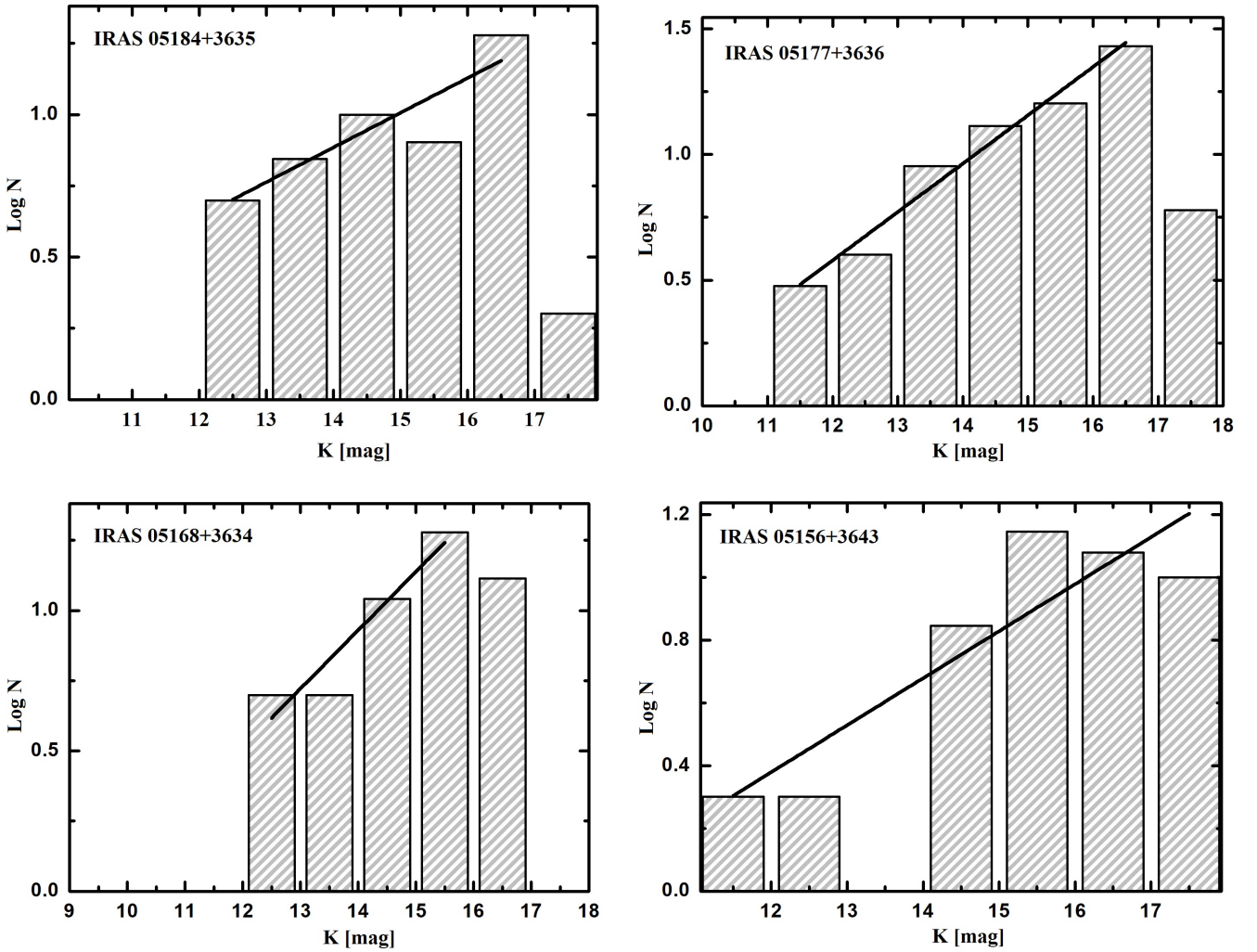


**Fig. 6.** K luminosity functions derived for the subregions as a histogram of the number of stars in logarithm vs. apparent K magnitude. The bin size corresponds to 1 mag. The linear fits are represented by the straight lines and the slopes obtained are given in each figure.

KLFs of young clusters. [Megeath et al. \(1996\)](#) found similar values of  $\alpha$  slopes around the W3 IRS 5 cluster ( $\alpha=0.24$ ), and that it is consistent with an age of 0.3 Myr with a Miller-Scalo IMF. [Ojha et al. \(2004\)](#) estimated the KLF slope of NGC 7538 to be  $\alpha=0.28 \pm 0.02$  and with an age of  $\sim 1$  Myr.

In addition, according to the calculation of [Massi et al. \(2000\)](#),  $\alpha$  values between 0.2 and 0.28 are consistent with an age range of 0.1–3 Myr. The  $\alpha$  values of the observable subregions are close to this range of values; therefore, the age of all four subregions can be estimated between 0.1 and 3 Myr, which

also closely reflects the location of stellar objects relative to the isochrones. The KLF of the IRAS 05156+3643 star-forming region differs from the other subregions, i.e., a sharp decline does not occur in the end, which means that in this case the KLF reflects the real picture of the subregion, and in the remaining cases the decline is abrupt, reflecting the completeness limit of the survey. The KLF of IRAS 05156+3643 star-forming region complicates the resolution of the  $\alpha$  slope value, but in any case it falls within the 0.15–0.28 range.

### 3.6. SED analysis

In order to learn about the evolutionary stages of the YSOs that have measured magnitudes in longer wavelengths, we constructed their spectral energy distributions (SEDs) and fitted them with the radiative transfer models of Robitaille et al. (2007). The models assume an accretion scenario in the star formation process where a central star is surrounded by an accretion disk, an infalling flattened envelope, and the presence of bipolar cavities. We used the command-line version of the SED fitting tool where a large number of precomputed models are available. The SEDs are constructed for 45 Class I and 75 Class II evolutionary stage YSOs. This procedure was done using wavelengths ranging from 1.1  $\mu\text{m}$  to 160  $\mu\text{m}$ , in particular J, H, and K (UKIDSS); 3.6 and 4.5  $\mu\text{m}$  (*S pitzer* IRAC); 3.4, 4.6, 12, and 22  $\mu\text{m}$  (WISE); 8.28, 12.13, 14.65, and 21.3  $\mu\text{m}$  (MSX); 12 and 25  $\mu\text{m}$  (IRAS); and 70 and 160  $\mu\text{m}$  (*Herschel* PACS). We took the apparent magnitudes of those surveys where the object was detected as a point source, i.e., we did not take data from the *Herschel* PACS extended source list and SPIRE 250,350,500  $\mu\text{m}$  surveys (all YSOs in the molecular cloud were detected as extended in the *Herschel* SPIRE survey). We also did not take the IRAS 60 and 100  $\mu\text{m}$  data, but instead we took the *Herschel* PACS Point Source Catalogs 70 and 160  $\mu\text{m}$  data, which provide better resolution than the IRAS 60 and 100  $\mu\text{m}$ . The SED fit was carried out using both distance estimations: 1.88 and 6.1 kpc. We used the ranges of the interstellar extinction ( $A_V$ ) and the distances of 1–40 mag, and 5.5–6.5 kpc and 1.6–2 kpc, respectively.

Figure 7 shows the constructed SEDs for those objects associated with IRAS sources in the near and far distances. To identify the representative values of different physical parameters, the tool retrieved the best fit model and all models for which the differences between their  $\chi^2$  values and the best  $\chi^2$  were smaller than  $3N$ , where  $N$  is the number of the data points used (as suggested in Robitaille et al. 2007). This approach was taken because the sampling of the model grid is too sparse to effectively determine the minima of the  $\chi^2$  surface and consequently obtain the confidence intervals.

Table 7 shows the weighted means and the standard deviations of parameters for all models with  $\chi^2 - \chi^2_{best} < 3N$  at near and far distances: 1.88 and 6.1 kpc. In Table 7, the members of subregions are separated from each other and the parameters of member of each subregion are listed in the following order: first, the received parameters of IRAS sources, then the parameters of MSX sources (if there is an identical object with any MSX source in that subregion). Next are the parameters of Class I objects, and finally those of Class II. The numbering of the objects was done according to Table 5.

According to the results of SED fitting tool at distances of 1.88 and 6.1 kpc, objects associated with IRAS and MSX sources can be classified as middle-mass YSOs (Table 7), which confirms the results obtained in the color-color and color-magnitude diagrams. The results of the SED fitting tool in general confirm the age estimations obtained by the KLF slope for

each subregion. The ratio between disk accretion and envelope infall rates of our objects correspond closely to those parameters given for Class I objects in Grave & Kumar (2009).

### 3.7. Substructures of molecular cloud

In this section, we give an overview of the substructures of four clearly visible subregions found in the molecular cloud. Figure 8 shows the local density (LD) distribution of selected YSOs ( $N = 240$ ) within the obtained radii (see Section 3.3) on the K-band images. A LD has been decided for each object on the surface with a radius equal to the distance to the closest  $n$ -th star. The value of LD for the first isodense exceeds the density of a field with a value of  $3\sigma$ . We investigate separately the substructures of subregions, and the distributions of Class I and Class II evolutionary stage objects in the subregions. Each of the subregions is an embedded cluster.

The LD distribution of all the YSOs in the subregions shows elongated structures. The elongated structure was also evident in some of the earlier studies of clusters (Carpenter et al. 1997; Hillenbrand & Hartmann 1998). The elongation appears to be a result of the primordial structure in the cloud, and the elongation is aligned with the filamentary structure seen in the parent molecular cloud (Allen et al. 2007) and they are often composed of subregions (Lada et al. 1996; Chen et al. 1997; Megeath & Wilson 1997; Allen et al. 2002). All subregions have an expressed elongation and each consists of subgroups.

Figure 8 (top left panel) shows the LD distribution of YSOs in the IRAS 05184+3635 star-forming region. The IRAS 05184+3635 star-forming region has a bimodal structure and the main concentration of objects is located  $\sim 40$  arcsec northwest (NW) of IRAS 05184+3635, which is associated with a MSX object (G170.8276+00.0098).

The LD distribution of YSOs in the IRAS 05177+3636 star-forming region is shown in Figure 8 (top right panel). The IRAS 05177+3636 star-forming region also has a bimodal structure and consists of two main subgroups, each with an elongation. There are three MSX sources in the IRAS 05177+3636 star-forming region, one of them (G170.7268-00.1012) is associated with IRAS 05177+3636. The second MSX source (G170.7196-00.1118) is located in the northeast (NE) subgroup with IRAS 05177+3636, and the third (G170.7247-00.1388) is in the second subgroup  $\sim 2.2$  arcmin to the southwest (SW) of IRAS 05177+3636. However, it should be noted that IRAS 05177+3636 and all the MSX sources are on the edges of two subgroups.

The LD distribution in IRAS 05168+3634 star-forming region demonstrates unique elongation (Figure 8, bottom left panel). There are no clearly visible subgroups, but three poles associated with MSX sources can be seen. One of the subgroups is located around IRAS 05168+3634, which is the dominant object in the given subgroup. IRAS 05168+3634 is identified with MSX G170.6575-00.2685. Another subgroup is found to the NE of IRAS 05168+3634. Molinari et al. (1998) detected 6 cm radio emission 102 arcsec away from IRAS 05168+3634 whose coordinates are  $\alpha_{2000}=05:20:23.53$ ,  $\delta_{2000}=+36:38:17.58$ .

The location of the second MSX G170.6589-00.2334 object is  $\sim 2.118$  arcmin NE of the position of IRAS 05168+3634. The third subgroup in the IRAS 05168+3634 star-forming region is located to the southeast (SE) of the IRAS 05168+3634.

The MSX G170.6758-00.2691 object in the IRAS 05168+3634 star-forming region is  $\sim 1.135$  arcmin SE of the position of IRAS 05168+3634 and is located in the subgroup. In the case of the IRAS 05168+3634 subregion

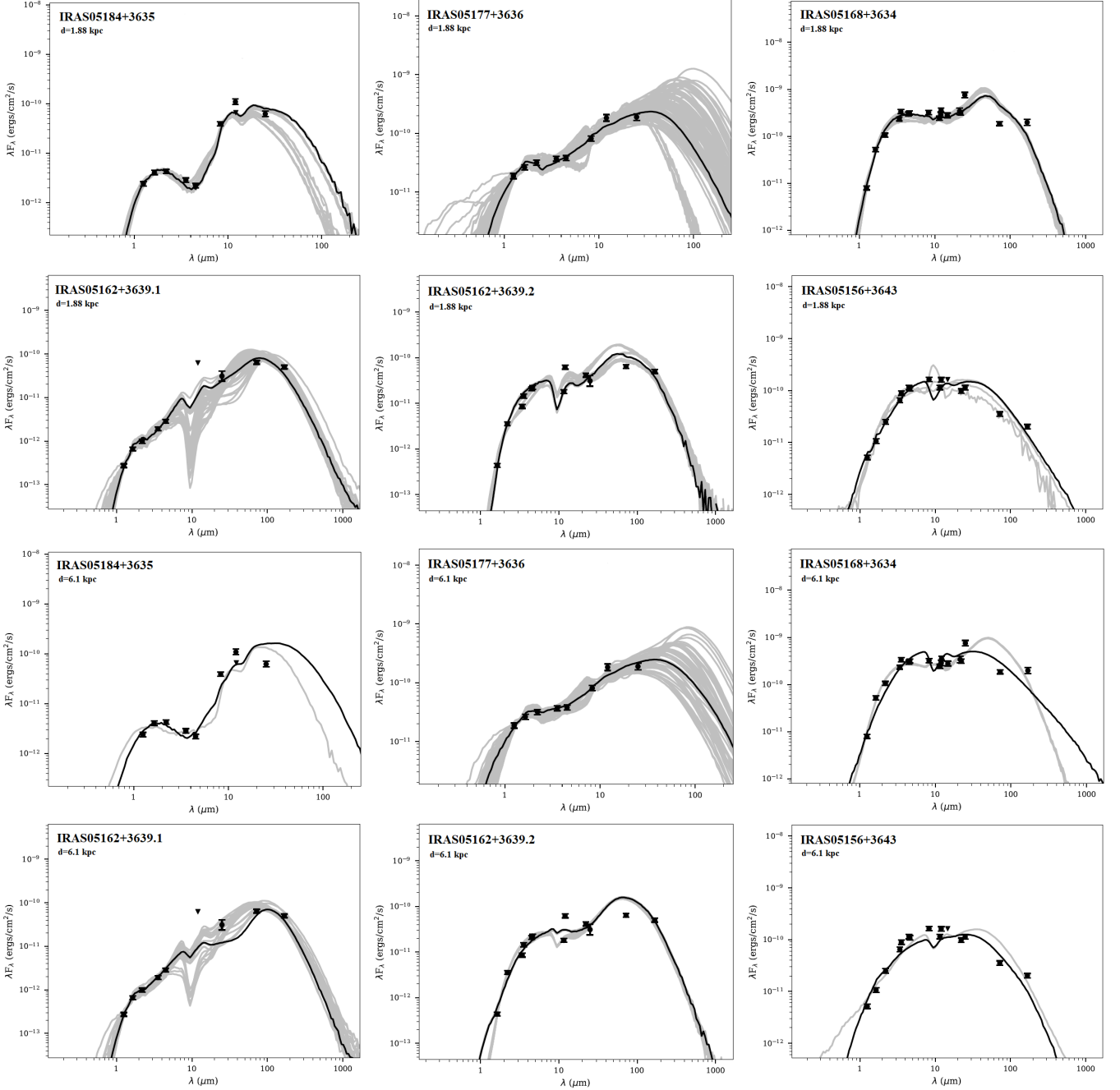


**Fig. 7.** Infrared SEDs of IRAS sources are fitted to the models of [Robitaille et al. \(2007\)](#) for distances of 1.88 and 6.1 kpc. The filled circles represent the input fluxes, while triangles represent upper limits from the respective clumps. The black line shows the best fitting model and gray lines show the subsequent good fits.

the IRAS and MSX sources are also located in the edges of subgroups.

The IRAS 05156+3643 star-forming region has the most complex structure (Figure 8, bottom right panel). It consists of three subgroups that show elongated structures, and one of them is even composed of two smaller subgroups. IRAS 05156+3643 is out of these three subgroups. This IRAS object is associated with MSX G170.3964-00.3827.

The LD distribution on the IRAS 05162+3639 star-forming region cannot provide any information because there are only five objects. It should be noted that all of these five objects were classified as Class I evolutionary stage objects (see text above), and that two of them were identified with IRAS 05162+3639.

This binary needs a separate study and it should be noted that the results obtained from the SED are likely to be incorrect.

If the observed morphologies of embedded clusters result from the filamentary and clumpy nature of the parental molecular clouds, then the younger Class 0/I objects, which have the least time to move away from their star formation sites, should show more pronounced structures than the older, PMS Class II and Class III stellar objects. However, there is no difference between the distributions of Class I and II objects in the field of the subregions, but there is a big difference between the distributions of Class I and II objects in the molecular cloud as a whole (Figure 3).



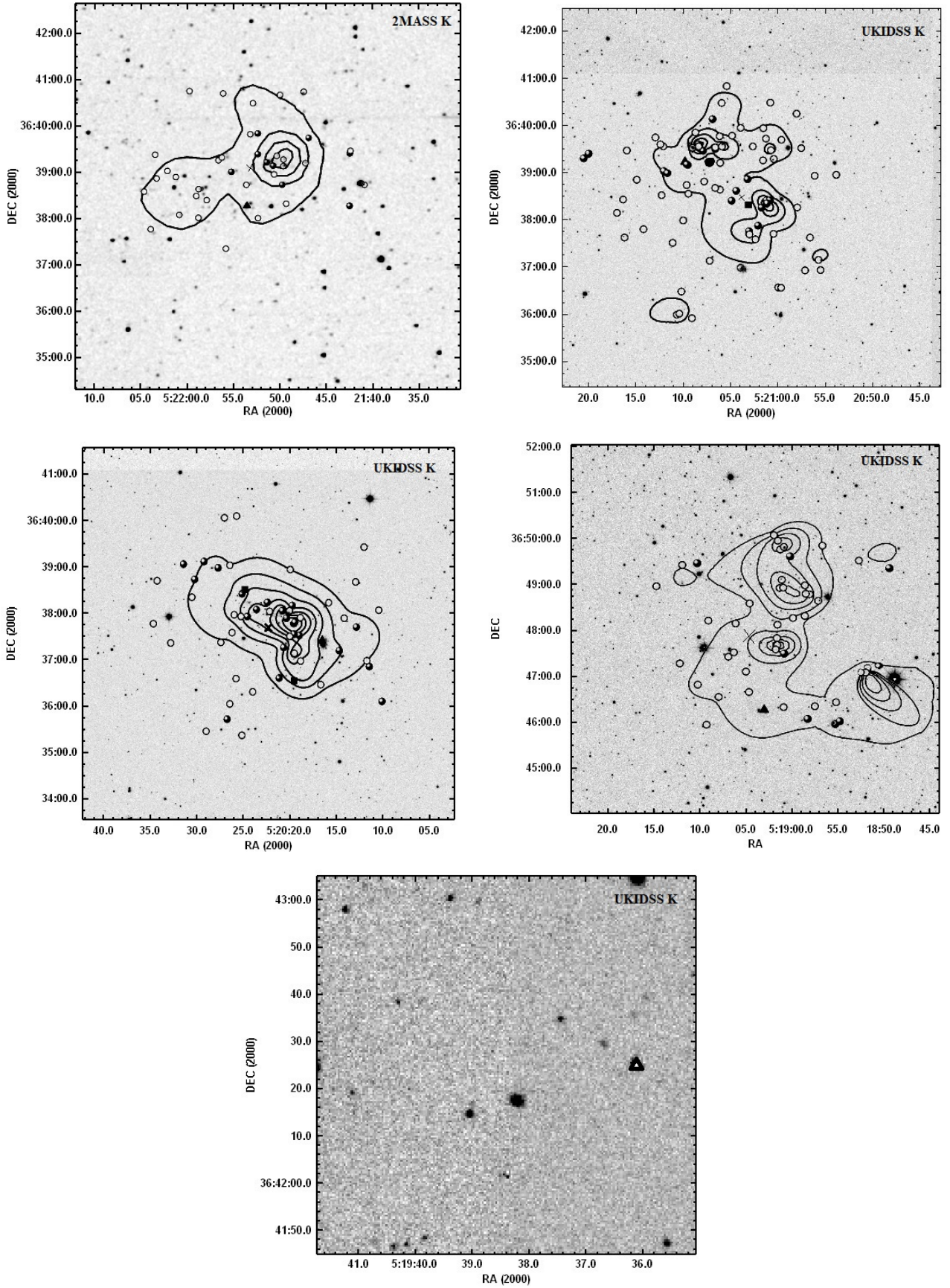


**Fig. 8.** LD distribution of the YSOs and spatial distribution of the Class I and Class II objects superposed on the K-band images. Filled and open circles represent the Class I and Class II objects, respectively. The triangles and squares show the location of IRAS and MSX sources, respectively, which are also classified as Class I objects. The geometric center of each subregion is indicated by a cross.

#### 4. Conclusion

Our investigations show that the IRAS 05168+3634 star-forming region, considered in previous studies, has a more complicated structure in the FIR wavelengths. Studies in FIR wavelengths suggest that the IRAS 05168+3634 star-forming region is located in a quite large molecular cloud within a region of approximately 24 arcmin radius (the center of the molecular cloud is conditionally selected as IRAS 05168+3634), which in turn consists of four additional star-forming regions. From the statistical analysis it follows that all IRAS star-forming regions are at the same distance: 6.1 kpc (Molinari et al. 1996) or 1.88 kpc (Sakai et al. 2012), i.e., there is a small probability that these star-forming regions may be the result of superposition. In addition, these regions repeat the shape of the molecular cloud. Also the distances of IRAS 05184+3635 and IRAS 05177+3636 assessed based on the  $^{13}\text{CO}$  velocities were evaluated at the same 1.4 kpc value, which coincides with the distance of IRAS 05168+3634 based on trigonometric parallax.

In this paper, we also analyzed the stellar content of the molecular cloud and separately for each star-forming region associated with IRAS sources using the J, H, K UKIDSS-DR6; [3.6], [4.5]  $\mu\text{m}$  *Spitzer* GLIMPSE 360; and [3.4], [4.6], [12], [22]  $\mu\text{m}$  ALLWISE survey images and photometric data to construct color-color and color-magnitude diagrams, which are useful tools for identifying YSO candidates. Using NIR and MIR photometric data, we obtain the census of the young stellar populations and their characteristics within a 24 arcmin radius region surrounding the molecular cloud, which includes 1224 candidate YSOs, 240 of which are concentrated around five IRAS sources. We classified 71 YSOs as evolutionary stage Class I objects and 132–169 YSOs (depending on the distance) as evolutionary stage Class II objects within the radii of subregions. One can see, depending on the color-color and color-magnitude diagrams, the number of Class II evolutionary stage objects is changing, but the number of Class I evolutionary stage objects is not changing, and the conclusion is that the selection of Class I objects is highly accurate. It should be noted that, unlike the Class II objects, the Class I objects are located mainly in the filaments of the molecular cloud, i.e., the distribution of Class I objects reflects the initial state of the parent molecular cloud. The estimated distances and the interstellar extinctions of each subregion were taken into account in the corrections of J and K magnitudes for the color-magnitude diagrams, which generates a great difference in the number of Class II objects. From the color-magnitude diagram analysis using evolutionary models of various ages by Siess et al. (2000), there is a large distribution of ages, but the age of most of them is on the order of  $10^5$  years. A mass completeness limit has been quoted for two distances. Selected YSOs located in the IRAS 05184+3635, IRAS 05168+3634, and IRAS 05156+3643 star-forming regions are explicitly targeted at a specific mass range for two distances; for objects in the IRAS 05177+3636 star-forming region there is no similar dependency. The members of the IRAS 05184+3635 and IRAS 05156+3643 subregions are targeted to a lower mass range, i.e., the members of IRAS 05184+3635 are distributed in the ranges of 0.3–1.5 and 0.8–5  $M_{\text{sun}}$  and the members of IRAS 05156+3643 in the ranges 0.2–1.6 and 0.6–3  $M_{\text{sun}}$  at distances of 1.88 and 6.1 kpc, respectively. Conversely, the members of the IRAS 05168+3634 subregion are distributed in a higher mass range, i.e., they are at 0.5–2.5 and 0.9–>7  $M_{\text{sun}}$  at distances of 1.88 and 6.1 kpc, respectively.

We have also calculated the slope of the KLFs for four subregions, namely IRAS 05184+3635, IRAS 05177+3636,

IRAS 05168+3634, and IRAS 05156+3643. The KLF of these subregions shows unusually low values for the  $\alpha$  slope: 0.12–0.21. According to the values of the slopes of the KLFs, the age of all four subregions can be estimated between 0.1 and 3 Myr. There are not enough YSOs within the radius of the IRAS 05162+3639 subregion, so the KLFs for this subregion were not constructed.

The SEDs were constructed for 45 and 75 YSOs with evolutionary stages Class I and Class II, respectively. This procedure was done using wavelengths ranging from 1.1  $\mu\text{m}$  to 160  $\mu\text{m}$ . According to the results of the SED fitting tool, IRAS 05184+3635, IRAS 05177+3636, and IRAS 05162+3639 can be classified as Class I for both distances. The sources IRAS 05168+3634 and IRAS 05156+3643 can be classified as flat-spectrum objects for both distances. At the distance of 6.1 kpc, all IRAS sources have 6–7  $M_{\text{sun}}$ , except for IRAS 05156+3643, and one of the two objects associated with the IRAS 05162+3639 binary object (both have 3  $M_{\text{sun}}$  mass). At the distance of 1.88 kpc, estimated masses vary considerably only in the case of IRAS 05184+3635 and IRAS 05177+3636, and the mass estimation is the highest for IRAS 05168+3634: 5  $M_{\text{sun}}$ . The results of the SED fitting tool, in general, are well correlated with the age estimations obtained by the KLF slope for each subregion. According to the results of the SED fitting tool, at distances of 1.88 and 6.1 kpc, IRAS and MSX sources can be classified as middle-mass YSOs, which confirms the results obtained in the color-color and color-magnitude diagrams.

All star-forming regions have complicated structures. They contained the subgroups, which are mainly associated with IRAS and MSX sources. The observed young subregions and parental molecular cloud morphologies are similar and elongated. This is particularly well expressed when only the youngest Class I/0 sources are considered. Perhaps the similarities in morphologies result from the distribution of fragmentation sites in the parent cloud. The Class I sources are often distributed along filamentary structures, while the Class II sources are more widely distributed. A similar distribution of Class II evolutionary stage objects can be explained by the fact that these objects have had enough time to leave their own birthplaces. In the case of Class I evolutionary stage objects, that time is small, and this is why they are located on the filaments of parent molecular cloud, thus they clearly reflect the initial state of the parent cloud.

*Acknowledgements.* I am very grateful to the anonymous referee for the helpful comments and suggestions. I thank my supervisor Dr. Elena Nikoghosyan for her support. This research has made use of the data obtained at UKIRT, which is supported by NASA and operated under an agreement among the University of Hawaii, the University of Arizona, and Lockheed Martin Advanced Technology Center; operations are enabled through the cooperation of the East Asian Observatory. We gratefully acknowledge the use of data from the NASA/IPAC Infrared Science Archive, which is operated by the Jet Propulsion Laboratory, California Institute of Technology, under contract with the National Aeronautics and Space Administration. I thank my colleagues in the GLIMPSE 360 *Spitzer* Legacy Surveys. This work was made possible by a research grant from the Armenian National Science and Education Fund (ANSEF) based in New York, USA.

#### References

- Ali, B. & Depoy, D. L. 1995, *AJ*, 109, 709
- Allen, L., Megeath, S. T., Gutermuth, R., et al. 2007, *Protostars and Planets V*, 361
- Allen, L. E., Myers, P. C., Di Francesco, J., et al. 2002, *ApJ*, 566, 993
- Azatyan, N. M., Nikoghosyan, E. H., & Khachatryan, K. G. 2016, *Astrophysics*, 59, 339
- Baug, T., Ojha, D. K., Dewangan, L. K., et al. 2015, *MNRAS*, 454, 4335

- Bessell, M. S. & Brett, J. M. 1988, *PASP*, 100, 1134
- Bohlin, R. C., Savage, B. D., & Drake, J. F. 1978, *ApJ*, 224, 132
- Bronfman, L., Nyman, L.-A., & May, J. 1996, *A&AS*, 115, 81
- Carpenter, J. M. 2001, *AJ*, 121, 2851
- Carpenter, J. M., Meyer, M. R., Dougados, C., Strom, S. E., & Hillenbrand, L. A. 1997, *AJ*, 114, 198
- Casoli, F., Dupraz, C., Gerin, M., Combes, F., & Boulanger, F. 1986, *A&A*, 169, 281
- Cesaroni, R., Massi, F., Arcidiacono, C., et al. 2015, *A&A*, 581, A124
- Chen, H., Tafalla, M., Greene, T. P., Myers, P. C., & Wilner, D. J. 1997, *ApJ*, 475, 163
- Churchwell, E., Babler, B. L., Meade, M. R., et al. 2009, *PASP*, 121, 213
- Di Francesco, J., Johnstone, D., Kirk, H., MacKenzie, T., & Ledwosinska, E. 2008, *ApJS*, 175, 277
- Dobashi, K. 2011, *PASJ*, 63, S1
- Egan, M. P., Price, S. D., Kraemer, K. E., et al. 2003, *VizieR Online Data Catalog*, 5114
- Faustini, F., Molinari, S., Testi, L., & Brand, J. 2009, *A&A*, 503, 801
- Fazio, G. G., Hora, J. L., Allen, L. E., et al. 2004, *ApJS*, 154, 10
- Flaherty, K. M., Pipher, J. L., Megeath, S. T., et al. 2007, *ApJ*, 663, 1069
- Fontani, F., Cesaroni, R., & Furuya, R. S. 2010, *A&A*, 517, A56
- Grave, J. M. C. & Kumar, M. S. N. 2009, *A&A*, 498, 147
- Griffin, M. J., Abergel, A., Abreu, A., et al. 2010, *A&A*, 518, L3
- Guan, X., Wu, Y., & Ju, B. 2008a, *MNRAS*, 391, 869
- Guan, X., Wu, Y., & Ju, B. 2008b, *MNRAS*, 391, 869
- Gutermuth, R. A., Pipher, J. L., Myers, P. C., et al. 2006, in *Bulletin of the American Astronomical Society*, Vol. 38, American Astronomical Society Meeting Abstracts #208, 87
- Harju, J., Lehtinen, K., Booth, R. S., & Zinchenko, I. 1998, *A&AS*, 132, 211
- Hartmann, L. 2009, *Accretion Processes in Star Formation: Second Edition* (Cambridge University Press)
- Hernández, J., Calvet, N., Hartmann, L., et al. 2005, *AJ*, 129, 856
- Hillenbrand, L. A. & Hartmann, L. W. 1998, *ApJ*, 492, 540
- Jose, J., Pandey, A. K., Ogura, K., et al. 2012, *MNRAS*, 424, 2486
- Kenyon, S. J., Gomez, M., Marzke, R. O., & Hartmann, L. 1994, *AJ*, 108, 251
- Koenig, X. P., Leisawitz, D. T., Benford, D. J., et al. 2012, *ApJ*, 744, 130
- Kumar, M. S. N., Keto, E., & Clerkin, E. 2006, *A&A*, 449, 1033
- Lada, C. J. & Adams, F. C. 1992, *ApJ*, 393, 278
- Lada, C. J., Alves, J., & Lada, E. A. 1996, *AJ*, 111, 1964
- Lada, C. J. & Lada, E. A. 2003, *ARA&A*, 41, 57
- Lada, C. J., Margulis, M., & Dearborn, D. 1984, *ApJ*, 285, 141
- Lada, E. A., Depoy, D. L., Evans, II, N. J., & Gatley, I. 1991, *ApJ*, 371, 171
- Lada, E. A. & Lada, C. J. 1995, *AJ*, 109, 1682
- Lépine, S. & Shara, M. M. 2005, *AJ*, 129, 1483
- López-Chico, T. & Salas, L. 2007, *Rev. Mexicana Astron. Astrofis.*, 43, 155
- Lucas, P. W., Hoare, M. G., Longmore, A., et al. 2008, *MNRAS*, 391, 136
- Maddox, N., Jarvis, M. J., Banerji, M., et al. 2017, *MNRAS*, 470, 2314
- Massi, F., Lorenzetti, D., Giannini, T., & Vitali, F. 2000, *A&A*, 353, 598
- Megeath, S. T., Herter, T., Beichman, C., et al. 1996, *A&A*, 307, 775
- Megeath, S. T. & Wilson, T. L. 1997, *AJ*, 114, 1106
- Meyer, M. R., Calvet, N., & Hillenbrand, L. A. 1997, *AJ*, 114, 288
- Molinari, S., Brand, J., Cesaroni, R., & Palla, F. 1996, *A&A*, 308, 573
- Molinari, S., Brand, J., Cesaroni, R., Palla, F., & Palumbo, G. G. C. 1998, *A&A*, 336, 339
- Neugebauer, G., Habing, H. J., van Duinen, R., et al. 1984, *ApJ*, 278, L1
- Ojha, D. K., Tamura, M., Nakajima, Y., et al. 2004, *ApJ*, 616, 1042
- Pilbratt, G. L., Riedinger, J. R., Passvogel, T., et al. 2010, *A&A*, 518, L1
- Poglitsch, A., Waelkens, C., Geis, N., et al. 2010, *A&A*, 518, L2
- Preibisch, T. 2012, *Research in Astronomy and Astrophysics*, 12, 1
- Rieke, G. H. & Lebofsky, M. J. 1985, *ApJ*, 288, 618
- Robitaille, T. P., Whitney, B. A., Indebetouw, R., & Wood, K. 2007, *ApJS*, 169, 328
- Ruiz-Velasco, A. E., Felli, D., Migenes, V., & Wiggins, B. K. 2016, *ApJ*, 822, 101
- Sakai, N., Honma, M., Nakanishi, H., et al. 2012, *PASJ*, 64, 108
- Schlegel, D. J., Finkbeiner, D. P., & Davis, M. 1998, *ApJ*, 500, 525
- Siess, L., Dufour, E., & Forestini, M. 2000, *A&A*, 358, 593
- Sunada, K., Nakazato, T., Ikeda, N., et al. 2007, *PASJ*, 59, 1185
- Varricatt, W. P., Davis, C. J., Ramsay, S., & Todd, S. P. 2010, *MNRAS*, 404, 661
- Wang, K., Wu, Y. F., Ran, L., Yu, W. T., & Miller, M. 2009, *A&A*, 507, 369
- Wouterloot, J. G. A. & Brand, J. 1989, *A&AS*, 80, 149
- Wright, E. L., Eisenhardt, P. R. M., Mainzer, A. K., et al. 2010, *AJ*, 140, 1868
- Yorke, H. W. & Sonnhalter, C. 2002, *ApJ*, 569, 846
- Zhang, Q., Hunter, T. R., Brand, J., et al. 2005, *ApJ*, 625, 864
- Zinnecker, H., McCaughrean, M. J., & Wilking, B. A. 1993, in *Protostars and Planets III*, ed. E. H. Levy & J. I. Lunine, 429–495



**Table 5.** Members of subregions with NIR and MIR photometry

ID	$\alpha(2000)$ (hh mm ss)	$\delta(2000)$ (dd mm ss)	J (mag)	H (mag)	K (mag)	[3.6] $\mu$ m (mag)	[4.5] $\mu$ m (mag)	W1 (mag)	W2 (mag)	W3 (mag)	W4 (mag)	Final/class
(1)	(2)	(3)	(4)	(5)	(6)	(7)	(8)	(9)	(10)	(11)	(12)	(13)
IRAS 05184+3635												
1	5 21 41.35	36 38 46.50	10.333 $\pm$ 0.000	10.642 $\pm$ 0.000	10.076 $\pm$ 0.000	9.595 $\pm$ 0.043	9.433 $\pm$ 0.040	10.109 $\pm$ 0.021	9.957 $\pm$ 0.018	9.098 $\pm$ 0.032	8.375 $\pm$ 0.294	Class II
2*	5 21 42.79	36 39 29.08	17.751 $\pm$ 0.036	17.182 $\pm$ 0.039	16.825 $\pm$ 0.056	16.146 $\pm$ 0.101	15.999 $\pm$ 0.109	–	–	–	–	Class II
3	5 22 1.21	36 39 3.86	16.155 $\pm$ 0.010	15.563 $\pm$ 0.008	15.213 $\pm$ 0.012	15.048 $\pm$ 0.063	14.866 $\pm$ 0.084	–	–	–	–	Class II
4*	5 21 46.99	36 39 45.13	17.678 $\pm$ 0.034	17.076 $\pm$ 0.036	16.725 $\pm$ 0.052	16.395 $\pm$ 0.093	16.174 $\pm$ 0.125	17.240 $\pm$ 0.181	17.229 $\pm$ 6.892	12.403 $\pm$ 4.961	8.745 $\pm$ 3.498	Class II
5	5 21 58.99	36 40 43.70	17.378 $\pm$ 0.024	16.752 $\pm$ 0.026	16.314 $\pm$ 0.032	15.994 $\pm$ 0.082	15.839 $\pm$ 0.087	–	–	–	–	Class II
6*	5 22 2.46	36 39 24.05	17.509 $\pm$ 0.030	16.869 $\pm$ 0.026	16.497 $\pm$ 0.039	15.819 $\pm$ 0.069	15.469 $\pm$ 0.070	–	–	–	–	Class II
7	5 21 55.61	36 40 40.58	17.113 $\pm$ 0.022	16.437 $\pm$ 0.018	15.973 $\pm$ 0.024	15.548 $\pm$ 0.073	15.374 $\pm$ 0.093	15.461 $\pm$ 0.048	15.052 $\pm$ 0.088	11.995 $\pm$ 4.798	8.569 $\pm$ 3.428	Class II
8	5 22 2.91	36 37 51.02	17.674 $\pm$ 0.035	16.958 $\pm$ 0.028	16.512 $\pm$ 0.039	16.049 $\pm$ 0.091	15.800 $\pm$ 0.067	16.150 $\pm$ 0.070	16.269 $\pm$ 0.229	12.345 $\pm$ 4.938	8.978 $\pm$ 3.591	Class II
9	5 22 2.30	36 38 54.28	17.899 $\pm$ 0.043	17.181 $\pm$ 0.035	16.773 $\pm$ 0.050	16.112 $\pm$ 0.079	15.852 $\pm$ 0.082	–	–	–	–	Class II
10	5 21 52.87	36 37 30.75	18.624 $\pm$ 0.083	17.897 $\pm$ 0.067	17.450 $\pm$ 0.093	16.877 $\pm$ 0.180	16.408 $\pm$ 0.083	–	–	–	–	Class II
11	5 21 52.09	36 38 5.11	17.541 $\pm$ 0.031	16.814 $\pm$ 0.025	16.406 $\pm$ 0.036	16.246 $\pm$ 0.069	16.024 $\pm$ 0.113	–	–	–	–	Class II
12	5 21 50.48	36 38 59.69	18.210 $\pm$ 0.054	17.428 $\pm$ 0.049	16.691 $\pm$ 0.050	16.225 $\pm$ 0.085	16.006 $\pm$ 0.120	–	–	–	–	Class II
13	5 21 58.10	36 38 5.36	18.051 $\pm$ 0.049	17.260 $\pm$ 0.037	16.695 $\pm$ 0.047	15.870 $\pm$ 0.053	15.494 $\pm$ 0.060	–	–	–	–	Class II
14	5 21 52.85	36 39 49.51	16.230 $\pm$ 0.010	15.427 $\pm$ 0.007	14.959 $\pm$ 0.010	14.333 $\pm$ 0.054	14.092 $\pm$ 0.046	14.735 $\pm$ 0.036	14.573 $\pm$ 0.067	12.297 $\pm$ 4.919	8.861 $\pm$ 3.544	Class II
15	5 21 58.07	36 38 41.04	14.709 $\pm$ 0.003	13.867 $\pm$ 0.002	13.378 $\pm$ 0.003	12.710 $\pm$ 0.042	12.459 $\pm$ 0.038	–	–	–	–	Class II
16	5 21 55.34	36 37 26.73	17.338 $\pm$ 0.026	16.496 $\pm$ 0.019	16.030 $\pm$ 0.026	15.737 $\pm$ 0.080	15.590 $\pm$ 0.054	15.461 $\pm$ 0.047	15.781 $\pm$ 0.156	11.427 $\pm$ 0.202	8.382 $\pm$ 0.350	Class II
17	5 21 47.50	36 40 42.53	14.327 $\pm$ 0.002	13.438 $\pm$ 0.002	12.831 $\pm$ 0.002	11.964 $\pm$ 0.035	11.572 $\pm$ 0.037	12.046 $\pm$ 0.023	11.507 $\pm$ 0.021	9.532 $\pm$ 0.058	7.826 $\pm$ 0.188	Class II
18	5 22 3.58	36 38 38.01	16.397 $\pm$ 0.012	15.502 $\pm$ 0.008	14.925 $\pm$ 0.010	14.152 $\pm$ 0.055	13.777 $\pm$ 0.043	13.895 $\pm$ 0.027	13.467 $\pm$ 0.033	12.364 $\pm$ 4.946	8.969 $\pm$ 3.588	Class II
19	5 21 54.58	36 41 13.34	18.888 $\pm$ 0.105	17.947 $\pm$ 0.070	17.277 $\pm$ 0.080	16.588 $\pm$ 0.130	16.267 $\pm$ 0.082	–	–	–	–	Class II
20	5 21 50.47	36 38 59.59	18.152 $\pm$ 0.054	17.209 $\pm$ 0.036	16.680 $\pm$ 0.047	16.225 $\pm$ 0.085	16.006 $\pm$ 0.120	–	–	–	–	Class II
21	5 21 57.26	36 38 27.37	18.152 $\pm$ 0.054	17.200 $\pm$ 0.035	16.644 $\pm$ 0.045	16.333 $\pm$ 0.131	16.164 $\pm$ 0.114	–	–	–	–	Class II
22	5 22 0.01	36 38 9.05	17.142 $\pm$ 0.022	16.145 $\pm$ 0.014	15.487 $\pm$ 0.016	14.666 $\pm$ 0.040	14.099 $\pm$ 0.043	14.861 $\pm$ 0.039	14.272 $\pm$ 0.049	11.713 $\pm$ 0.327	8.313 $\pm$ 3.325	Class II
23	5 21 52.60	36 40 28.29	16.813 $\pm$ 0.017	15.810 $\pm$ 0.010	15.173 $\pm$ 0.012	14.829 $\pm$ 0.064	14.487 $\pm$ 0.093	15.084 $\pm$ 0.042	15.107 $\pm$ 0.099	12.579 $\pm$ 5.032	8.984 $\pm$ 3.594	Class II
24	5 21 49.27	36 38 22.94	17.863 $\pm$ 0.040	16.851 $\pm$ 0.029	16.127 $\pm$ 0.030	14.957 $\pm$ 0.055	14.397 $\pm$ 0.047	14.514 $\pm$ 0.034	13.705 $\pm$ 0.038	10.220 $\pm$ 0.091	7.808 $\pm$ 0.211	Class II
25	5 21 49.26	36 38 22.92	17.919 $\pm$ 0.044	16.887 $\pm$ 0.027	16.120 $\pm$ 0.028	14.957 $\pm$ 0.055	14.397 $\pm$ 0.047	14.514 $\pm$ 0.034	13.705 $\pm$ 0.038	10.220 $\pm$ 0.091	7.808 $\pm$ 0.211	Class II
26	5 21 42.87	36 38 20.27	19.231 $\pm$ 0.136	18.132 $\pm$ 0.093	16.893 $\pm$ 0.060	14.354 $\pm$ 0.042	13.487 $\pm$ 0.043	14.912 $\pm$ 0.040	13.537 $\pm$ 0.034	10.542 $\pm$ 0.102	7.906 $\pm$ 0.184	Class I
27	5 21 56.08	36 39 17.04	17.602 $\pm$ 0.033	16.457 $\pm$ 0.018	15.714 $\pm$ 0.019	15.156 $\pm$ 0.059	14.875 $\pm$ 0.061	–	–	–	–	Class II
28	5 21 49.89	36 40 38.79	17.945 $\pm$ 0.045	16.784 $\pm$ 0.025	15.812 $\pm$ 0.021	14.916 $\pm$ 0.113	14.531 $\pm$ 0.130	–	–	–	–	Class II
29	5 21 55.72	36 39 20.40	15.894 $\pm$ 0.008	14.728 $\pm$ 0.004	14.122 $\pm$ 0.005	13.337 $\pm$ 0.043	12.790 $\pm$ 0.036	13.373 $\pm$ 0.035	12.674 $\pm$ 0.031	10.578 $\pm$ 0.135	6.531 $\pm$ 0.106	Class II
30	5 21 49.89	36 40 38.76	17.998 $\pm$ 0.045	16.749 $\pm$ 0.027	15.791 $\pm$ 0.022	14.916 $\pm$ 0.113	14.531 $\pm$ 0.130	–	–	–	–	Class II
31	5 21 53.22	36 38 20.43	15.480 $\pm$ 0.006	14.171 $\pm$ 0.003	13.283 $\pm$ 0.003	12.294 $\pm$ 0.040	11.839 $\pm$ 0.045	–	–	–	–	Class II/I
32	5 21 53.27	36 38 46.47	15.855 $\pm$ 0.008	14.528 $\pm$ 0.004	13.868 $\pm$ 0.004	13.273 $\pm$ 0.057	13.120 $\pm$ 0.048	13.202 $\pm$ 0.026	12.880 $\pm$ 0.031	8.402 $\pm$ 0.035	5.301 $\pm$ 0.045	Class II
33	5 21 42.85	36 39 25.82	18.691 $\pm$ 0.083	17.362 $\pm$ 0.046	16.309 $\pm$ 0.035	15.300 $\pm$ 0.059	14.624 $\pm$ 0.049	–	–	–	–	Class I
34	5 21 47.31	36 39 13.54	17.508 $\pm$ 0.029	16.168 $\pm$ 0.016	14.859 $\pm$ 0.010	13.418 $\pm$ 0.039	12.593 $\pm$ 0.037	13.116 $\pm$ 0.025	12.223 $\pm$ 0.024	10.214 $\pm$ 0.075	8.625 $\pm$ 0.481	Class I
35	5 21 53.54	36 40 4.15	18.986 $\pm$ 0.115	17.617 $\pm$ 0.052	16.731 $\pm$ 0.048	16.262 $\pm$ 0.108	16.043 $\pm$ 0.094	–	–	–	–	Class II
36	5 21 49.54	36 39 18.09	16.768 $\pm$ 0.015	15.353 $\pm$ 0.008	14.419 $\pm$ 0.007	13.265 $\pm$ 0.063	12.797 $\pm$ 0.035	–	–	–	–	Class II
37	5 21 50.20	36 39 22.73	16.904 $\pm$ 0.017	15.441 $\pm$ 0.008	14.285 $\pm$ 0.006	13.086 $\pm$ 0.047	12.536 $\pm$ 0.053	–	–	–	–	Class II
38	5 21 50.20	36 39 22.70	16.883 $\pm$ 0.018	15.415 $\pm$ 0.007	14.269 $\pm$ 0.006	13.086 $\pm$ 0.047	12.536 $\pm$ 0.053	–	–	–	–	Class II
39	5 21 49.55	36 39 10.02	15.301 $\pm$ 0.005	13.823 $\pm$ 0.002	12.872 $\pm$ 0.002	11.897 $\pm$ 0.029	11.530 $\pm$ 0.035	12.166 $\pm$ 0.023	11.556 $\pm$ 0.022	9.748 $\pm$ 0.052	6.318 $\pm$ 0.091	Class II
40	5 21 49.54	36 39 18.05	16.827 $\pm$ 0.017	15.338 $\pm$ 0.007	14.425 $\pm$ 0.007	13.265 $\pm$ 0.063	12.797 $\pm$ 0.035	–	–	–	–	Class II
41	5 21 49.54	36 39 9.98	15.306 $\pm$ 0.005	13.810 $\pm$ 0.002	12.870 $\pm$ 0.002	11.897 $\pm$ 0.029	11.530 $\pm$ 0.035	12.166 $\pm$ 0.023	11.556 $\pm$ 0.022	9.748 $\pm$ 0.052	6.318 $\pm$ 0.091	Class II
42	5 22 0.37	36 38 56.22	15.421 $\pm$ 0.005	13.909 $\pm$ 0.002	12.673 $\pm$ 0.002	11.213 $\pm$ 0.045	10.744 $\pm$ 0.030	11.615 $\pm$ 0.023	10.846 $\pm$ 0.020	8.649 $\pm$ 0.030	6.592 $\pm$ 0.085	Class II
43	5 21 58.31	36 38 32.62	16.313 $\pm$ 0.011	14.742 $\pm$ 0.004	13.766 $\pm$ 0.004	12.815 $\pm$ 0.051	12.409 $\pm$ 0.034	–	–	–	–	Class II
44	5 21 52.10	36 39 24.75	18.948 $\pm$ 0.111	17.354 $\pm$ 0.041	16.000 $\pm$ 0.025	14.313 $\pm$ 0.046	13.373 $\pm$ 0.042	–	–	–	–	Class I
45	5 21 53.26	36 39 24.74	18.990 $\pm$ 0.115	17.295 $\pm$ 0.039	16.007 $\pm$ 0.025	15.254 $\pm$ 0.066	15.043 $\pm$ 0.061	15.426 $\pm$ 0.052	14.656 $\pm$ 0.069	12.302 $\pm$ 4.921	7.804 $\pm$ 0.201	Class II
46	5 21 49.65	36 38 46.61	17.146 $\pm$ 0.021	15.304 $\pm$ 0.007	13.654 $\pm$ 0.004	11.123 $\pm$ 0.031	10.285 $\pm$ 0.030	11.916 $\pm$ 0.023	10.538 $\pm$ 0.021	7.895 $\pm$ 0.022	5.368 $\pm$ 0.040	Class I
47	5 21 49.65	36 38 46.56	17.145 $\pm$ 0.022	15.285 $\pm$ 0.007	13.659 $\pm$ 0.004	11.123 $\pm$ 0.031	10.285 $\pm$ 0.030	11.916 $\pm$ 0.023	10.538 $\pm$ 0.021	7.895 $\pm$ 0.022	5.368 $\pm$ 0.040	Class I
48	5 21 52.10	36 39 50.58	19.190 $\pm$ 0.139	17.061 $\pm$ 0.032	15.824 $\pm$ 0.022	15.104 $\pm$ 0.056	14.911 $\pm$ 0.075	15.527 $\pm$ 0.053	15.743 $\pm$ 0.180	12.250 $\pm$ 4.900	8.616 $\pm$ 3.446	Class I
49	5 21 50.58	36 39 10.51	18.345 $\pm$ 0.061	16.189 $\pm$ 0.016	14.747 $\pm$ 0.009	13.834 $\pm$ 0.061	13.356 $\pm$ 0.059	–	–	–	–	Class I
50	5 21 50.57	36 39 10.44	18.490 $\pm$ 0.074	16.139 $\pm$ 0.014	14.718 $\pm$ 0.008	13.834 $\pm$ 0.061	13.356 $\pm$ 0.059	–	–	–	–	Class I
51	5 21 51.21	36 39 14.61	16.981 $\pm$ 0.019	14.537 $\pm$ 0.004	12.548 $\pm$ 0.002	10.473 $\pm$ 0.109	9.452 $\pm$ 0.043	10.668 $\pm$ 0.021	9.184 $\pm$ 0.019	7.097 $\pm$ 0.016	4.285 $\pm$ 0.031	Class I
52	5 21 54.77	36 39 2.78	18.119 $\pm$ 0.052	15.658 $\pm$ 0.009	13.771 $\pm$ 0.004	12.012 $\pm$ 0.031	10.961 $\pm$ 0.033	12.585 $\pm$ 0.024	11.005 $\pm$ 0.020	8.086 $\pm$ 0.023	4.992 $\pm$ 0.039	Class I
IRAS 05177+3636												

59*	5 21 19.82	36 38 13.97	17.183 ± 0.022	16.647 ± 0.024	16.254 ± 0.034	15.934 ± 0.088	15.797 ± 0.095	—	—	—	—	Class II
60	5 20 57.35	36 39 39.30	13.396 ± 0.001	12.845 ± 0.001	12.526 ± 0.002	—	—	12.232 ± 0.024	12.086 ± 0.023	8.714 ± 0.035	7.141 ± 0.141	Class II
61*	5 21 5.58	36 36 56.21	17.489 ± 0.028	16.933 ± 0.031	16.604 ± 0.047	16.235 ± 0.085	16.025 ± 0.073	—	—	—	—	Class II
62*	5 20 54.53	36 40 12.86	17.044 ± 0.019	16.480 ± 0.021	16.169 ± 0.031	16.048 ± 0.075	15.857 ± 0.062	16.094 ± 0.067	16.613 ± 6.645	12.373 ± 4.949	8.765 ± 3.506	Class II
63*	5 21 0.81	36 40 32.39	17.843 ± 0.039	17.249 ± 0.042	16.874 ± 0.059	16.621 ± 0.095	16.396 ± 0.059	—	—	—	—	Class II
64*	5 20 49.42	36 39 14.36	17.732 ± 0.035	17.137 ± 0.038	16.757 ± 0.053	16.425 ± 0.106	16.230 ± 0.067	—	—	—	—	Class II
65*	5 21 18.65	36 37 34.02	17.172 ± 0.021	16.569 ± 0.023	16.235 ± 0.033	15.874 ± 0.080	15.743 ± 0.069	—	—	—	—	Class II
66*	5 20 56.94	36 40 14.57	17.769 ± 0.036	17.155 ± 0.038	16.807 ± 0.056	16.604 ± 0.109	16.398 ± 0.082	—	—	—	—	Class II
67	5 20 56.14	36 39 55.77	17.133 ± 0.021	16.506 ± 0.021	16.134 ± 0.030	15.881 ± 0.075	15.723 ± 0.055	—	—	—	—	Class II
68*	5 20 50.16	36 37 33.85	17.905 ± 0.041	17.276 ± 0.043	16.942 ± 0.063	16.482 ± 0.084	16.241 ± 0.103	—	—	—	—	Class II
69	5 21 13.15	36 40 5.39	16.869 ± 0.016	16.228 ± 0.017	15.792 ± 0.022	15.333 ± 0.074	15.227 ± 0.069	—	—	—	—	Class II
70	5 21 15.76	36 37 47.52	17.099 ± 0.020	16.451 ± 0.020	16.082 ± 0.029	15.829 ± 0.076	15.558 ± 0.068	—	—	—	—	Class II
71	5 21 11.26	36 37 25.21	16.604 ± 0.013	15.936 ± 0.013	15.551 ± 0.018	15.275 ± 0.072	15.106 ± 0.044	15.518 ± 0.051	15.751 ± 0.157	12.412 ± 4.965	8.837 ± 3.535	Class II
72	5 21 7.78	36 40 24.44	18.093 ± 0.048	17.398 ± 0.048	16.704 ± 0.051	16.026 ± 0.071	15.754 ± 0.061	16.164 ± 0.070	16.408 ± 0.269	12.056 ± 4.822	8.223 ± 0.300	Class II
73	5 20 55.69	36 39 41.96	16.555 ± 0.013	15.837 ± 0.012	15.370 ± 0.015	15.071 ± 0.058	14.913 ± 0.042	—	—	—	—	Class II
74	5 21 2.11	36 40 19.64	16.591 ± 0.013	15.869 ± 0.012	15.404 ± 0.016	15.021 ± 0.048	14.812 ± 0.041	15.132 ± 0.040	14.896 ± 0.071	12.342 ± 4.937	8.865 ± 3.546	Class II
75	5 20 55.78	36 37 39.92	17.686 ± 0.034	16.958 ± 0.032	16.562 ± 0.045	16.327 ± 0.090	16.098 ± 0.072	15.686 ± 0.052	15.395 ± 0.104	12.112 ± 4.845	8.495 ± 3.398	Class II
76	5 20 54.61	36 36 12.15	16.954 ± 0.018	16.206 ± 0.016	15.741 ± 0.021	15.511 ± 0.058	15.327 ± 0.052	—	—	—	—	Class II
77	5 21 3.71	36 41 12.90	16.382 ± 0.011	15.585 ± 0.009	14.979 ± 0.011	13.970 ± 0.039	13.358 ± 0.025	—	—	—	—	Class II
78	5 21 0.83	36 36 44.86	17.863 ± 0.039	17.053 ± 0.035	16.492 ± 0.042	16.041 ± 0.074	15.882 ± 0.056	15.917 ± 0.063	16.543 ± 0.298	12.014 ± 4.806	8.950 ± 0.502	Class II
79	5 20 58.54	36 37 31.33	15.594 ± 0.006	14.773 ± 0.005	14.301 ± 0.006	13.991 ± 0.049	13.849 ± 0.025	13.968 ± 0.028	13.822 ± 0.037	12.209 ± 4.884	8.784 ± 3.514	Class II
80	5 20 51.52	36 39 59.32	17.405 ± 0.026	16.577 ± 0.023	16.109 ± 0.030	15.800 ± 0.084	15.645 ± 0.058	—	—	—	—	Class II
81	5 21 13.89	36 40 16.47	18.290 ± 0.058	17.451 ± 0.050	16.859 ± 0.058	16.488 ± 0.085	16.243 ± 0.088	—	—	—	—	Class II
82	5 21 2.98	36 41 40.15	14.580 ± 0.003	13.726 ± 0.002	13.243 ± 0.003	12.504 ± 0.032	12.057 ± 0.021	12.630 ± 0.024	12.028 ± 0.024	10.064 ± 0.078	8.374 ± 0.296	Class II
83	5 21 3.71	36 41 12.88	16.383 ± 0.011	15.502 ± 0.009	14.920 ± 0.011	13.970 ± 0.039	13.358 ± 0.025	—	—	—	—	Class II
84	5 21 9.64	36 38 1.80	16.431 ± 0.011	15.509 ± 0.009	14.979 ± 0.011	14.595 ± 0.053	14.473 ± 0.038	14.748 ± 0.039	14.851 ± 0.073	12.350 ± 4.940	8.936 ± 3.574	Class II
85	5 21 8.95	36 39 31.86	13.200 ± 0.001	12.266 ± 0.001	11.562 ± 0.001	9.956 ± 0.080	9.307 ± 0.084	—	—	—	—	Class I
86	5 20 46.12	36 39 15.97	18.165 ± 0.052	17.226 ± 0.041	16.607 ± 0.047	16.202 ± 0.078	16.063 ± 0.066	—	—	—	—	Class II
87	5 20 57.58	36 38 22.67	16.647 ± 0.014	15.645 ± 0.010	14.954 ± 0.011	13.610 ± 0.044	12.907 ± 0.033	—	—	—	—	Class I
88	5 21 4.03	36 40 18.54	14.783 ± 0.003	13.779 ± 0.002	13.268 ± 0.003	12.526 ± 0.062	12.091 ± 0.025	12.633 ± 0.024	12.078 ± 0.023	10.316 ± 0.103	7.934 ± 0.251	Class II
89	5 20 58.94	36 40 2.17	16.041 ± 0.008	15.023 ± 0.006	14.406 ± 0.007	—	—	13.522 ± 0.027	12.709 ± 0.026	11.108 ± 0.192	8.678 ± 3.471	Class II
90	5 21 10.65	36 35 28.49	18.070 ± 0.047	17.051 ± 0.035	16.207 ± 0.033	15.317 ± 0.087	14.776 ± 0.096	—	—	—	—	Class II
91	5 21 4.72	36 38 54.39	14.920 ± 0.004	13.891 ± 0.002	13.340 ± 0.003	12.457 ± 0.033	12.186 ± 0.021	12.722 ± 0.026	12.295 ± 0.024	10.437 ± 0.098	8.082 ± 0.302	Class II
92	5 21 24.93	36 39 42.65	15.336 ± 0.005	14.301 ± 0.003	13.533 ± 0.003	12.380 ± 0.094	11.560 ± 0.077	12.571 ± 0.024	11.281 ± 0.022	8.774 ± 0.030	4.432 ± 0.025	Class I
93	5 21 4.71	36 40 0.58	14.217 ± 0.002	13.173 ± 0.001	12.704 ± 0.002	12.346 ± 0.045	12.116 ± 0.025	12.128 ± 0.023	11.583 ± 0.021	9.202 ± 0.034	5.680 ± 0.045	Class II
94	5 21 16.79	36 39 7.70	16.945 ± 0.018	15.889 ± 0.012	15.270 ± 0.014	14.988 ± 0.060	14.821 ± 0.053	14.965 ± 0.040	14.890 ± 0.077	12.441 ± 4.976	8.560 ± 3.424	Class II
95	5 21 10.25	36 35 30.38	17.434 ± 0.027	16.375 ± 0.019	15.408 ± 0.016	14.264 ± 0.080	13.684 ± 0.068	14.064 ± 0.029	13.333 ± 0.034	9.806 ± 0.061	7.117 ± 0.108	Class II
96	5 21 9.08	36 39 32.79	14.382 ± 0.002	13.296 ± 0.001	12.526 ± 0.002	—	—	9.150 ± 0.017	7.888 ± 0.012	5.066 ± 0.009	2.889 ± 0.015	Class I
97	5 21 9.39	36 39 37.12	13.255 ± 0.001	12.152 ± 0.001	11.104 ± 0.001	9.519 ± 0.035	8.751 ± 0.023	—	—	—	—	Class I
98	5 21 8.84	36 38 45.20	15.811 ± 0.007	14.702 ± 0.004	13.987 ± 0.005	13.537 ± 0.043	13.358 ± 0.039	13.713 ± 0.028	13.493 ± 0.033	12.417 ± 4.967	8.720 ± 3.488	Class II
99	5 20 59.77	36 39 8.53	18.982 ± 0.108	17.869 ± 0.074	16.880 ± 0.060	15.980 ± 0.071	15.240 ± 0.046	—	—	—	—	Class I
100	5 20 59.52	36 37 44.48	18.519 ± 0.071	17.396 ± 0.048	16.731 ± 0.052	16.405 ± 0.099	16.229 ± 0.088	—	—	—	—	Class I
101	5 20 59.62	36 38 26.75	12.763 ± 0.001	11.637 ± 0.001	10.542 ± 0.001	9.307 ± 0.040	8.477 ± 0.021	9.665 ± 0.023	8.408 ± 0.018	5.389 ± 0.012	3.031 ± 0.019	Class I
102	5 21 18.90	36 38 35.75	17.363 ± 0.025	16.170 ± 0.016	15.352 ± 0.015	14.480 ± 0.059	14.141 ± 0.073	14.374 ± 0.034	14.121 ± 0.050	10.105 ± 0.073	7.973 ± 3.189	Class II
103	5 21 3.97	36 39 35.15	15.310 ± 0.005	14.104 ± 0.003	13.286 ± 0.003	11.965 ± 0.048	11.599 ± 0.023	11.973 ± 0.024	11.159 ± 0.021	8.888 ± 0.031	4.845 ± 0.032	Class II
104	5 21 3.70	36 40 2.05	16.841 ± 0.016	15.632 ± 0.010	14.791 ± 0.009	13.822 ± 0.039	13.298 ± 0.026	13.799 ± 0.028	13.021 ± 0.028	10.525 ± 0.108	7.168 ± 0.122	Class II
105	5 21 4.70	36 39 57.62	17.306 ± 0.024	16.091 ± 0.015	15.388 ± 0.016	13.590 ± 0.052	12.866 ± 0.033	—	—	—	—	Class I
106	5 21 5.10	36 40 46.39	19.817 ± 0.232	18.598 ± 0.144	17.590 ± 0.114	16.133 ± 0.088	15.494 ± 0.052	—	—	—	—	Class I
107	5 21 8.31	36 35 22.66	19.150 ± 0.126	17.928 ± 0.078	17.044 ± 0.070	16.041 ± 0.098	15.801 ± 0.106	—	—	—	—	Class II
108	5 20 55.03	36 36 12.86	18.773 ± 0.089	17.523 ± 0.054	16.778 ± 0.055	16.524 ± 0.096	16.211 ± 0.067	—	—	—	—	Class II
109	5 21 9.10	36 38 59.38	16.448 ± 0.012	15.156 ± 0.006	14.334 ± 0.006	13.890 ± 0.045	13.674 ± 0.029	14.034 ± 0.030	13.660 ± 0.035	12.465 ± 4.986	8.171 ± 3.268	Class II
110	5 21 7.28	36 40 2.19	16.081 ± 0.009	14.761 ± 0.005	14.076 ± 0.005	13.269 ± 0.050	12.912 ± 0.023	13.013 ± 0.026	12.280 ± 0.025	10.069 ± 0.062	6.864 ± 0.093	Class II
111	5 20 48.86	36 36 57.60	18.697 ± 0.084	17.320 ± 0.045	16.474 ± 0.041	16.091 ± 0.078	15.859 ± 0.074	—	—	—	—	Class II
112	5 20 56.84	36 38 34.50	16.674 ± 0.014	15.240 ± 0.007	13.883 ± 0.004	11.927 ± 0.080	10.907 ± 0.043	—	—	—	—	Class I
113	5 21 7.27	36 40 5.43	18.124 ± 0.050	16.663 ± 0.025	15.633 ± 0.019	14.096 ± 0.061	13.598 ± 0.029	—	—	—	—	Class I
114	5 21 6.44	36 39 4.90	19.379 ± 0.155	17.903 ± 0.076	17.004 ± 0.067	16.491 ± 0.083	16.254 ± 0.068	—	—	—	—	Class II
115	5 20 48.56	36 36 41.30	19.044 ± 0.115	17.560 ± 0.056	16.434 ± 0.040	15.676 ± 0.094	15.349 ± 0.057	—	—	—	—	Class II
116	5 20 56.33	36 38 34.12	18.753 ± 0.088	17.232 ± 0.041	15.988 ± 0.027	14.666 ± 0.066	13.973 ± 0.048	—	—	—	—	Class I
117	5 21 12.70	36 40 1.84	17.406 ± 0.026	15.870 ± 0.012	14.981 ± 0.011	14.280 ± 0.051	13.869 ± 0.038	14.615 ± 0.033	14.181 ± 0.046	12.493 ± 4.997	8.752 ± 3.501	Class II
118	5 20 50.91	36 36 40.72	19.331 ± 0.149	17.767 ± 0.067	16.651 ± 0.049	16.105 ± 0.104	15.588 ± 0.057	15.943 ± 0.060	15.823 ± 0.149	12.579 ± 5.032	8.380 ± 3.352	Class II
119	5 21 8.22	36 39 59.67	17.106 ± 0.020	15.538 ± 0.009	14.584 ± 0.008	13.959 ± 0.046	13.789 ± 0.031	14.199 ± 0.032	13.582 ± 0.037	11.604 ± 0.286	6.892 ± 0.094	Class II
120	5 20 59.50	36 37 39.10	19.222 ± 0.134	17.642 ± 0.060	16.654 ± 0.049	16.039 ± 0.089	15.769 ± 0.065	—	—	—	—	Class II
121	5 21 12.99	36 38 42.80	17.806 ± 0.037	16.118 ± 0.015	15.101 ± 0.012	14.510 ± 0.048	14.347 ± 0.038	14.841 ± 0.041	14.614 ± 0.066	12.430 ± 4.972	8.156 ± 0.417	Class II
122	5 21 18.31	36 39 55.50	16.695 ± 0.014	14.862 ± 0.005	13.763 ± 0.004	13.203 ± 0.050	12.853 ± 0.040	13.400 ± 0.025	12.936 ± 0.028	12.409 ± 4.964	8.768 ± 3.507	Class II
123	5 21 2.19	36 38 33.63	19.339 ± 0.150	17.468 ± 0.051	16.337 ± 0.036	15.742 ± 0.066	15.482 ± 0.069	16.263 ± 0.079	15.955 ± 0.183	12.491 ± 4.996	7.977 ± 0.223	Class I
124	5 21 24.16	36 39 50.17	18.625 ± 0.078	16.674 ± 0.025	15.412 ± 0.016	14.774 ± 0.054	14.535 ± 0.041	—	—	—	—	Class I
125	5 21 1.49	36 38 49.98	17.760 ± 0.036	15.807 ± 0.011	14.741 ± 0.009	—	—	13.299				

127	5 20 58.12	36 37 53.43	19.054 ± 0.115	16.971 ± 0.032	15.803 ± 0.023	15.126 ± 0.069	14.899 ± 0.044	–	–	–	–	Class I
128	5 21 5.50	36 39 37.26	15.548 ± 0.006	13.454 ± 0.002	11.405 ± 0.001	9.270 ± 0.038	8.271 ± 0.022	9.443 ± 0.024	8.042 ± 0.020	5.306 ± 0.014	2.747 ± 0.017	Class I
129	5 21 12.60	36 39 21.83	–	16.586 ± 0.023	13.800 ± 0.004	10.828 ± 0.037	9.760 ± 0.022	11.219 ± 0.032	9.516 ± 0.021	7.407 ± 0.020	4.801 ± 0.061	Class I
130	5 21 12.05	36 39 18.55	–	–	17.596 ± 0.115	13.560 ± 0.047	11.784 ± 0.024	14.469 ± 0.285	11.592 ± 0.058	8.067 ± 0.030	3.449 ± 0.022	Class I
131	5 21 6.60	36 39 55.02	–	16.423 ± 0.020	14.843 ± 0.010	13.409 ± 0.046	12.927 ± 0.031	13.560 ± 0.030	12.469 ± 0.028	10.390 ± 0.081	5.166 ± 0.038	Class I
IRAS 05168+3634												
132*	5 20 20.20	36 37 59.90	10.460 ± 0.000	10.817 ± 0.000	10.191 ± 0.000	10.071 ± 0.042	10.024 ± 0.020	9.845 ± 0.021	9.679 ± 0.017	9.000 ± 0.035	3.247 ± 0.008	Class II
133**	5 20 15.70	36 38 11.00	17.765 ± 0.043	17.262 ± 0.042	16.923 ± 0.064	16.408 ± 0.094	16.128 ± 0.105	–	–	–	–	Class II
134*	5 20 11.59	36 39 27.50	16.382 ± 0.013	15.831 ± 0.012	15.510 ± 0.018	15.376 ± 0.068	15.168 ± 0.070	–	–	–	–	Class II
135**	5 20 26.28	36 40 10.41	17.761 ± 0.042	17.142 ± 0.038	16.714 ± 0.053	16.448 ± 0.075	16.258 ± 0.083	–	–	–	–	Class II
136**	5 20 25.70	36 35 7.78	17.433 ± 0.032	16.783 ± 0.027	16.423 ± 0.041	16.189 ± 0.086	15.862 ± 0.092	16.388 ± 0.098	15.972 ± 0.202	12.449 ± 4.980	8.851 ± 3.540	Class II
137*	5 20 35.90	36 37 41.83	17.206 ± 0.026	16.470 ± 0.021	15.945 ± 0.026	15.299 ± 0.068	14.884 ± 0.043	15.197 ± 0.043	14.810 ± 0.076	12.003 ± 4.801	8.350 ± 0.522	Class II
138*	5 20 20.10	36 38 56.48	17.772 ± 0.043	17.009 ± 0.033	16.573 ± 0.046	16.213 ± 0.087	16.082 ± 0.074	–	–	–	–	Class II
139*	5 20 29.81	36 35 13.37	16.996 ± 0.022	16.227 ± 0.017	15.724 ± 0.022	14.710 ± 0.049	14.146 ± 0.039	15.056 ± 0.040	14.593 ± 0.065	11.798 ± 4.719	8.538 ± 3.415	Class II
140	5 20 35.46	36 38 41.09	14.934 ± 0.004	14.164 ± 0.003	13.718 ± 0.004	13.280 ± 0.036	12.917 ± 0.025	13.422 ± 0.039	12.996 ± 0.037	11.189 ± 0.192	8.547 ± 3.419	Class II
141*	5 20 24.45	36 36 7.61	17.021 ± 0.022	16.218 ± 0.016	15.732 ± 0.022	15.178 ± 0.057	15.005 ± 0.045	–	–	–	–	Class II
142*	5 20 26.36	36 36 25.79	17.190 ± 0.026	16.382 ± 0.019	15.913 ± 0.026	15.512 ± 0.072	15.181 ± 0.051	15.840 ± 0.062	17.121 ± 6.848	12.120 ± 4.848	8.763 ± 3.505	Class II
143	5 20 18.97	36 36 34.19	13.522 ± 0.002	12.712 ± 0.001	12.172 ± 0.001	–	–	11.086 ± 0.021	10.354 ± 0.020	7.375 ± 0.017	3.053 ± 0.019	Class II
144*	5 20 33.88	36 37 15.21	17.906 ± 0.048	17.078 ± 0.036	16.570 ± 0.046	16.165 ± 0.083	16.019 ± 0.057	–	–	–	–	Class II
145*	5 20 28.11	36 37 15.88	17.693 ± 0.040	16.864 ± 0.029	16.369 ± 0.039	16.066 ± 0.091	15.798 ± 0.066	–	–	–	–	Class II
146	5 20 12.56	36 38 39.47	15.335 ± 0.006	14.496 ± 0.004	14.033 ± 0.005	13.169 ± 0.042	12.735 ± 0.027	13.399 ± 0.025	12.837 ± 0.028	11.018 ± 0.153	8.641 ± 3.456	Class II
147	5 20 27.69	36 40 8.26	16.677 ± 0.016	15.782 ± 0.011	15.289 ± 0.015	14.974 ± 0.047	14.829 ± 0.038	15.139 ± 0.041	15.182 ± 0.102	12.198 ± 4.879	8.357 ± 3.343	Class II
148	5 20 16.59	36 36 17.77	18.804 ± 0.110	17.839 ± 0.072	17.129 ± 0.077	16.071 ± 0.100	15.738 ± 0.092	–	–	–	–	Class II
149	5 20 13.90	36 37 49.56	16.185 ± 0.011	15.207 ± 0.007	14.488 ± 0.007	13.749 ± 0.039	13.293 ± 0.036	13.690 ± 0.027	12.898 ± 0.029	10.298 ± 0.094	8.665 ± 3.466	Class II
150	5 20 11.29	36 36 50.58	17.747 ± 0.042	16.738 ± 0.026	16.157 ± 0.032	15.796 ± 0.081	15.652 ± 0.079	–	–	–	–	Class II
151	5 20 20.55	36 37 49.25	17.041 ± 0.022	15.993 ± 0.013	15.220 ± 0.014	13.969 ± 0.058	13.241 ± 0.062	–	–	–	–	Class I
152	5 20 26.82	36 37 29.47	18.177 ± 0.062	17.104 ± 0.036	16.453 ± 0.042	15.910 ± 0.080	15.737 ± 0.074	–	–	–	–	Class II
153	5 20 19.63	36 37 1.02	17.073 ± 0.023	15.963 ± 0.013	15.288 ± 0.015	14.818 ± 0.062	14.605 ± 0.065	–	–	–	–	Class II
154	5 20 9.91	36 38 0.47	18.247 ± 0.066	17.113 ± 0.037	16.386 ± 0.040	15.886 ± 0.077	15.709 ± 0.110	–	–	–	–	Class II
155	5 20 25.67	36 38 23.10	16.781 ± 0.018	15.607 ± 0.010	14.657 ± 0.009	13.459 ± 0.050	12.781 ± 0.037	–	–	–	–	Class I
156	5 20 22.49	36 37 59.04	14.409 ± 0.003	13.157 ± 0.001	12.403 ± 0.002	11.689 ± 0.133	11.134 ± 0.084	–	–	–	–	Class II
157	5 20 31.43	36 38 18.54	17.353 ± 0.029	16.072 ± 0.014	15.320 ± 0.015	14.860 ± 0.056	14.725 ± 0.043	–	–	–	–	Class II
158	5 20 25.79	36 37 51.90	18.875 ± 0.116	17.575 ± 0.056	16.742 ± 0.054	16.180 ± 0.093	15.992 ± 0.100	–	–	–	–	Class II
159	5 20 21.40	36 36 26.66	15.650 ± 0.007	14.325 ± 0.003	13.401 ± 0.003	12.218 ± 0.044	11.578 ± 0.025	12.091 ± 0.022	11.423 ± 0.023	9.512 ± 0.048	5.023 ± 0.029	Class I
160	5 20 26.58	36 37 54.16	16.574 ± 0.015	15.185 ± 0.007	14.228 ± 0.006	12.833 ± 0.043	12.417 ± 0.025	13.354 ± 0.026	12.548 ± 0.026	10.265 ± 0.081	8.707 ± 3.483	Class II
161	5 20 27.09	36 35 50.87	19.067 ± 0.138	17.639 ± 0.059	16.585 ± 0.047	16.027 ± 0.107	15.574 ± 0.057	15.888 ± 0.066	15.681 ± 0.162	11.958 ± 4.783	8.029 ± 3.212	Class II
162	5 20 14.46	36 37 4.70	14.643 ± 0.003	13.170 ± 0.001	11.977 ± 0.001	9.930 ± 0.049	9.061 ± 0.027	10.137 ± 0.022	8.885 ± 0.020	6.353 ± 0.017	3.314 ± 0.021	Class I
163	5 20 16.46	36 36 42.03	17.414 ± 0.031	15.940 ± 0.013	15.069 ± 0.012	14.164 ± 0.041	13.793 ± 0.045	–	–	–	–	Class II
164	5 20 18.94	36 37 50.41	15.565 ± 0.007	14.079 ± 0.003	13.033 ± 0.002	11.913 ± 0.042	11.459 ± 0.040	11.695 ± 0.022	10.991 ± 0.020	9.292 ± 0.048	6.300 ± 0.088	Class II
165	5 20 19.89	36 38 6.82	17.969 ± 0.051	16.470 ± 0.021	15.219 ± 0.014	13.632 ± 0.052	13.035 ± 0.040	–	–	–	–	Class I
166	5 20 17.40	36 36 56.46	17.944 ± 0.050	16.312 ± 0.018	15.298 ± 0.015	14.734 ± 0.056	14.441 ± 0.055	–	–	–	–	Class II
167	5 20 18.91	36 36 50.13	18.338 ± 0.072	16.647 ± 0.024	15.627 ± 0.020	15.200 ± 0.067	14.934 ± 0.057	–	–	–	–	Class II
168	5 20 11.01	36 36 42.80	18.304 ± 0.070	16.602 ± 0.023	15.054 ± 0.012	13.294 ± 0.040	12.481 ± 0.029	13.824 ± 0.028	12.605 ± 0.028	10.259 ± 0.079	7.340 ± 0.174	Class I
169	5 20 20.18	36 37 24.49	16.980 ± 0.021	15.262 ± 0.007	14.182 ± 0.006	13.149 ± 0.038	12.664 ± 0.029	–	–	–	–	Class II
170	5 20 27.07	36 39 2.70	18.750 ± 0.103	16.965 ± 0.032	15.890 ± 0.025	15.352 ± 0.068	15.134 ± 0.045	15.504 ± 0.051	14.774 ± 0.070	11.884 ± 4.754	7.607 ± 0.159	Class II
171	5 20 30.05	36 39 7.69	17.945 ± 0.050	16.010 ± 0.014	14.815 ± 0.010	14.168 ± 0.041	13.941 ± 0.032	14.491 ± 0.034	13.997 ± 0.050	12.494 ± 4.998	8.125 ± 3.250	Class I
172	5 20 31.12	36 38 42.97	19.042 ± 0.135	17.095 ± 0.036	16.039 ± 0.029	15.362 ± 0.061	15.211 ± 0.052	15.651 ± 0.051	16.175 ± 0.217	12.212 ± 4.885	8.623 ± 3.449	Class I
173	5 20 25.05	36 37 51.82	17.977 ± 0.051	16.023 ± 0.014	14.756 ± 0.009	13.681 ± 0.046	13.114 ± 0.040	13.929 ± 0.030	13.067 ± 0.031	11.360 ± 0.218	8.564 ± 3.426	Class I
174	5 20 28.42	36 38 59.11	15.580 ± 0.007	13.584 ± 0.002	12.543 ± 0.002	11.993 ± 0.039	11.814 ± 0.023	12.159 ± 0.024	11.851 ± 0.024	11.592 ± 0.283	8.337 ± 3.335	Class I
175	5 20 21.00	36 37 59.66	15.934 ± 0.009	13.937 ± 0.002	12.669 ± 0.002	11.280 ± 0.049	10.800 ± 0.035	–	–	–	–	Class I
176	5 20 19.08	36 37 25.70	18.950 ± 0.125	16.912 ± 0.031	15.574 ± 0.019	14.443 ± 0.072	13.889 ± 0.039	–	–	–	–	Class I
177	5 20 25.33	36 38 28.84	17.685 ± 0.040	15.598 ± 0.009	13.911 ± 0.005	11.645 ± 0.068	9.749 ± 0.023	12.209 ± 0.024	9.497 ± 0.021	4.758 ± 0.014	1.701 ± 0.010	Class I
178	5 20 27.40	36 35 29.80	16.371 ± 0.013	14.233 ± 0.003	12.730 ± 0.002	11.330 ± 0.037	10.536 ± 0.022	11.658 ± 0.023	10.453 ± 0.021	8.312 ± 0.025	6.183 ± 0.063	Class I
179	5 20 9.53	36 35 54.38	18.830 ± 0.113	16.560 ± 0.023	14.797 ± 0.010	12.586 ± 0.041	11.575 ± 0.036	12.839 ± 0.024	11.568 ± 0.022	8.786 ± 0.033	6.723 ± 0.097	Class I
180	5 20 19.69	36 37 27.04	18.864 ± 0.115	16.514 ± 0.021	15.353 ± 0.016	14.377 ± 0.052	13.945 ± 0.037	–	–	–	–	Class I
181	5 20 12.48	36 37 37.00	19.186 ± 0.155	16.835 ± 0.029	15.585 ± 0.019	14.974 ± 0.057	14.723 ± 0.053	–	–	–	–	Class I
182	5 20 19.63	36 36 22.94	18.410 ± 0.076	15.895 ± 0.012	13.195 ± 0.003	9.521 ± 0.042	8.308 ± 0.025	9.884 ± 0.020	7.997 ± 0.019	4.914 ± 0.011	2.323 ± 0.012	Class I
183	5 20 16.44	36 37 18.70	14.183 ± 0.002	11.404 ± 0.000	9.804 ± 0.000	7.124 ± 0.038	6.516 ± 0.024	7.661 ± 0.030	6.374 ± 0.025	3.827 ± 0.015	1.397 ± 0.014	Class I
184	5 20 20.86	36 37 8.90	18.445 ± 0.079	15.629 ± 0.010	14.202 ± 0.006	13.410 ± 0.036	13.238 ± 0.023	–	–	–	–	Class I
185	5 20 32.42	36 39 4.10	18.602 ± 0.090	15.725 ± 0.011	14.198 ± 0.006	13.321 ± 0.039	13.115 ± 0.028	13.722 ± 0.027	13.155 ± 0.031	12.540 ± 5.016	8.884 ± 3.554	Class I
186	5 20 22.74	36 38 11.34	19.385 ± 0.185	16.348 ± 0.018	14.729 ± 0.009	13.536 ± 0.046	12.927 ± 0.038	–	–	–	–	Class I
187	5 20 24.00	36 38 1.51	–	18.043 ± 0.086	16.428 ± 0.041	13.897 ± 0.106	12.975 ± 0.083	14.086 ± 0.039	12.262 ± 0.035	9.392 ± 0.054	4.314 ± 0.034	Class I
188	5 20 19.57	36 37 43.80	–	17.574 ± 0.056	15.247 ± 0.014	13.643 ± 0.071	12.772 ± 0.042	13.106 ± 0.028	11.462 ± 0.023	10.026 ± 0.095	5.657 ± 0.035	Class I
IRAS 05162+3639												
189	5 19 30.83	36 43 55.65	19.135 ± 0.085	17.471 ± 0.039	16.083 ± 0.028	15.175 ± 0.075	14.515 ± 0.074	15.334 ± 0.050	14.406 ± 0.059	10.613 ± 0.123	8.050 ± 0.288	Class I
190	5 19 41.76	36 42 24.60	17.844 ± 0.042	16.148 ± 0.017	14.870 ± 0.010	12.730 ± 0.038	11.554 ± 0.031	–	–	–	–	Class I



191	5 19 41.15	36 44 37.62	–	17.893 ± 0.084	16.458 ± 0.041	14.803 ± 0.056	13.905 ± 0.047	15.197 ± 0.044	14.032 ± 0.047	10.772 ± 0.138	8.501 ± 0.389	Class I
192	5 19 42.00	36 42 30.04	–	16.593 ± 0.025	13.480 ± 0.003	10.537 ± 0.035	9.390 ± 0.040	11.251 ± 0.023	9.238 ± 0.021	6.639 ± 0.015	3.588 ± 0.015	Class I
193	5 19 46.13	36 43 13.58	–	17.523 ± 0.059	16.489 ± 0.042	15.550 ± 0.089	14.865 ± 0.079	15.613 ± 0.057	14.960 ± 0.081	11.386 ± 0.229	8.402 ± 0.423	Class I
IRAS 05156+3643												
194*	5 19 12.35	36 49 36.47	16.273 ± 0.007	15.878 ± 0.010	15.637 ± 0.019	15.442 ± 0.073	15.270 ± 0.073	15.507 ± 0.047	15.482 ± 0.120	12.385 ± 4.954	8.424 ± 3.370	Class II
195*	5 18 53.30	36 47 7.94	16.714 ± 0.010	16.193 ± 0.012	15.925 ± 0.024	15.660 ± 0.076	15.444 ± 0.108	–	–	–	–	Class II
196*	5 19 2.22	36 47 45.32	17.365 ± 0.017	16.827 ± 0.022	16.409 ± 0.037	16.106 ± 0.095	15.929 ± 0.096	–	–	–	–	Class II
197*	5 18 52.57	36 47 14.34	17.451 ± 0.019	16.910 ± 0.024	16.540 ± 0.041	16.069 ± 0.077	15.824 ± 0.108	–	–	–	–	Class II
198*	5 19 1.56	36 49 4.99	18.066 ± 0.032	17.513 ± 0.041	17.074 ± 0.068	16.736 ± 0.124	16.600 ± 0.117	–	–	–	–	Class II
199*	5 18 57.85	36 48 46.99	18.302 ± 0.039	17.728 ± 0.050	17.285 ± 0.082	16.886 ± 0.152	16.487 ± 0.111	–	–	–	–	Class II
200*	5 19 10.70	36 46 50.54	18.114 ± 0.034	17.537 ± 0.042	17.182 ± 0.075	16.679 ± 0.120	16.477 ± 0.141	–	–	–	–	Class II
201	5 18 57.38	36 50 3.22	16.362 ± 0.008	15.771 ± 0.009	15.436 ± 0.016	15.292 ± 0.089	15.048 ± 0.096	14.721 ± 0.038	14.793 ± 0.075	12.418 ± 4.967	8.952 ± 3.581	Class II
202	5 19 1.73	36 49 16.24	16.752 ± 0.011	16.143 ± 0.012	15.806 ± 0.022	15.337 ± 0.074	15.110 ± 0.070	15.128 ± 0.039	15.727 ± 0.149	11.993 ± 4.797	8.792 ± 3.517	Class II
203	5 19 9.56	36 48 19.44	17.230 ± 0.016	16.621 ± 0.018	16.212 ± 0.031	15.993 ± 0.079	15.674 ± 0.093	–	–	–	–	Class II
204	5 19 5.22	36 46 40.29	17.109 ± 0.014	16.490 ± 0.016	16.165 ± 0.030	15.894 ± 0.073	15.744 ± 0.082	15.660 ± 0.056	14.784 ± 0.072	12.285 ± 4.914	7.845 ± 0.251	Class II
205	5 18 59.17	36 48 56.82	16.673 ± 0.010	16.044 ± 0.011	15.604 ± 0.018	15.363 ± 0.066	15.184 ± 0.079	–	–	–	–	Class II
206	5 19 12.61	36 47 19.92	18.141 ± 0.035	17.503 ± 0.041	17.037 ± 0.066	16.670 ± 0.127	16.259 ± 0.118	–	–	–	–	Class II
207	5 18 58.77	36 48 55.83	16.993 ± 0.013	16.319 ± 0.014	15.908 ± 0.024	15.759 ± 0.074	15.551 ± 0.066	–	–	–	–	Class II
208	5 18 59.27	36 48 26.00	18.013 ± 0.031	17.334 ± 0.035	16.820 ± 0.054	16.583 ± 0.084	16.355 ± 0.092	–	–	–	–	Class II
209	5 19 6.63	36 48 15.58	16.681 ± 0.010	16.001 ± 0.011	15.628 ± 0.019	15.500 ± 0.068	15.263 ± 0.082	15.078 ± 0.039	15.180 ± 0.091	11.870 ± 4.748	8.823 ± 3.529	Class II
210	5 18 53.51	36 49 42.67	18.168 ± 0.035	17.477 ± 0.040	17.110 ± 0.070	16.725 ± 0.118	16.603 ± 0.112	–	–	–	–	Class II
211	5 19 0.52	36 48 23.20	16.050 ± 0.006	15.347 ± 0.006	14.919 ± 0.010	14.734 ± 0.051	14.551 ± 0.065	14.800 ± 0.034	14.948 ± 0.079	12.478 ± 4.991	8.765 ± 3.506	Class II
212	5 19 1.97	36 49 4.66	18.379 ± 0.042	17.674 ± 0.048	17.287 ± 0.082	16.828 ± 0.122	16.708 ± 0.145	–	–	–	–	Class II
213	5 18 52.77	36 47 7.32	17.026 ± 0.013	16.278 ± 0.013	15.634 ± 0.018	14.655 ± 0.046	14.095 ± 0.061	14.532 ± 0.033	14.069 ± 0.042	12.215 ± 4.886	8.964 ± 3.586	Class II
214	5 18 59.27	36 49 8.53	16.649 ± 0.010	15.842 ± 0.009	15.400 ± 0.015	15.171 ± 0.060	15.002 ± 0.062	–	–	–	–	Class II
215	5 19 5.15	36 48 43.47	19.481 ± 0.114	18.644 ± 0.116	17.815 ± 0.134	16.850 ± 0.110	16.496 ± 0.118	–	–	–	–	Class II
216	5 19 1.48	36 50 1.59	17.747 ± 0.024	16.903 ± 0.024	16.274 ± 0.033	15.807 ± 0.082	15.354 ± 0.102	–	–	–	–	Class II
217	5 19 2.15	36 50 10.28	18.787 ± 0.061	17.894 ± 0.058	17.169 ± 0.074	16.345 ± 0.111	16.125 ± 0.106	–	–	–	–	Class II
218	5 19 10.75	36 49 38.97	18.068 ± 0.032	17.161 ± 0.030	15.943 ± 0.025	13.716 ± 0.053	12.738 ± 0.035	14.030 ± 0.037	12.774 ± 0.029	9.965 ± 0.065	7.564 ± 0.179	Class I
219	5 19 0.83	36 49 48.31	13.885 ± 0.002	12.958 ± 0.001	12.202 ± 0.001	10.715 ± 0.028	9.591 ± 0.058	11.000 ± 0.023	9.762 ± 0.021	6.491 ± 0.016	4.228 ± 0.022	Class I
220	5 19 2.38	36 47 39.53	17.349 ± 0.017	16.397 ± 0.015	15.823 ± 0.022	15.483 ± 0.066	15.317 ± 0.083	–	–	–	–	Class II
221	5 19 7.41	36 47 29.26	15.728 ± 0.005	14.746 ± 0.004	14.161 ± 0.005	13.820 ± 0.045	13.483 ± 0.045	–	–	–	–	Class II
222	5 18 51.34	36 47 15.71	18.485 ± 0.046	17.484 ± 0.040	16.913 ± 0.058	14.934 ± 0.094	13.998 ± 0.055	–	–	–	–	Class I
223	5 19 2.57	36 50 17.73	19.033 ± 0.076	17.964 ± 0.062	17.067 ± 0.068	16.507 ± 0.128	16.031 ± 0.096	–	–	–	–	Class II
224	5 19 8.48	36 46 33.48	18.703 ± 0.057	17.618 ± 0.045	16.575 ± 0.043	15.751 ± 0.101	15.411 ± 0.076	–	–	–	–	Class II
225	5 19 1.52	36 46 19.54	15.822 ± 0.005	14.706 ± 0.004	14.016 ± 0.005	12.939 ± 0.036	12.428 ± 0.034	13.217 ± 0.025	12.334 ± 0.025	9.593 ± 0.049	5.790 ± 0.037	Class II
226	5 18 55.95	36 46 26.10	17.840 ± 0.026	16.718 ± 0.020	16.072 ± 0.027	15.734 ± 0.085	15.486 ± 0.088	–	–	–	–	Class II
227	5 19 6.83	36 47 35.49	12.942 ± 0.001	11.788 ± 0.001	11.003 ± 0.001	10.604 ± 0.034	10.476 ± 0.030	10.799 ± 0.022	10.499 ± 0.021	10.422 ± 0.097	8.994 ± 3.598	Class II
228	5 19 9.74	36 45 55.09	16.899 ± 0.012	15.623 ± 0.008	14.772 ± 0.009	13.824 ± 0.041	13.310 ± 0.035	14.123 ± 0.030	13.405 ± 0.033	10.917 ± 0.148	8.248 ± 3.299	Class II
229	5 19 1.88	36 49 58.01	17.800 ± 0.025	16.441 ± 0.016	15.618 ± 0.018	15.144 ± 0.059	14.954 ± 0.071	–	–	–	–	Class II
230	5 19 5.53	36 47 8.66	19.707 ± 0.140	18.325 ± 0.086	16.898 ± 0.058	16.041 ± 0.093	15.551 ± 0.075	–	–	–	–	Class II
231	5 19 2.23	36 47 55.04	19.008 ± 0.074	17.571 ± 0.043	16.667 ± 0.047	16.350 ± 0.101	16.161 ± 0.090	–	–	–	–	Class II
232	5 19 1.47	36 47 33.64	17.614 ± 0.022	16.121 ± 0.012	14.256 ± 0.006	12.840 ± 0.054	11.710 ± 0.037	12.813 ± 0.024	11.022 ± 0.022	7.881 ± 0.022	4.879 ± 0.026	Class I
233	5 18 58.20	36 46 20.51	18.047 ± 0.031	16.534 ± 0.017	15.551 ± 0.017	15.085 ± 0.057	14.886 ± 0.062	15.521 ± 0.047	15.364 ± 0.101	12.353 ± 4.941	8.465 ± 3.386	Class II
234	5 19 3.62	36 46 15.68	14.644 ± 0.002	13.128 ± 0.001	11.364 ± 0.001	8.553 ± 0.033	7.541 ± 0.021	9.051 ± 0.022	7.530 ± 0.021	4.630 ± 0.014	2.655 ± 0.018	Class I
235	5 19 15.09	36 49 7.01	19.399 ± 0.107	17.879 ± 0.057	16.722 ± 0.050	15.847 ± 0.068	15.516 ± 0.092	–	–	–	–	Class II
236	5 18 50.23	36 49 32.09	20.325 ± 0.245	18.765 ± 0.128	17.829 ± 0.134	15.935 ± 0.087	14.873 ± 0.063	16.072 ± 0.076	14.953 ± 0.080	12.067 ± 0.425	8.469 ± 3.388	Class I
237	5 19 2.17	36 48 13.68	17.374 ± 0.018	15.643 ± 0.008	14.640 ± 0.008	14.233 ± 0.071	13.953 ± 0.061	14.450 ± 0.032	14.177 ± 0.052	12.156 ± 4.862	8.646 ± 3.458	Class II
238	5 18 56.01	36 45 55.86	19.821 ± 0.154	17.615 ± 0.044	15.311 ± 0.014	12.656 ± 0.054	11.758 ± 0.050	–	–	–	–	Class I
239	5 18 55.53	36 45 59.84	16.678 ± 0.010	14.230 ± 0.002	12.089 ± 0.001	9.922 ± 0.041	8.950 ± 0.036	10.167 ± 0.024	8.886 ± 0.021	6.745 ± 0.017	4.196 ± 0.022	Class I
240	5 18 58.96	36 46 2.92	19.860 ± 0.160	16.504 ± 0.016	14.455 ± 0.007	13.338 ± 0.046	12.812 ± 0.041	13.853 ± 0.028	12.783 ± 0.026	12.137 ± 4.855	7.455 ± 0.132	Class I

**Notes.** (1)-ID number in final list of sub-region members, (2),(3)-The position is taken from the UKIDSS survey, (4)-(12)-apparent magnitudes with errors, (13)-Classification of YSOs according to color-color diagrams W1-W4 are four WISE survey bands, (\*) - objects that are located to the left of ZAMS in one color - magnitude diagram, (\*\*) - objects that are located to the left of ZAMS in both color - magnitude diagrams

**Table 6.** Members of subregions with FIR photometry

ID	Name	[8.28] $\mu\text{m}$ (mJy)	[12.13] $\mu\text{m}$ (mJy)	[14.65] $\mu\text{m}$ (mJy)	[21.3] $\mu\text{m}$ (mJy)	[12] $\mu\text{m}$ (mJy)	[25] $\mu\text{m}$ (mJy)	[60] $\mu\text{m}$ (mJy)	[100] $\mu\text{m}$ (mJy)	[70] $\mu\text{m}$ (mJy)	[160] $\mu\text{m}$ (mJy)	[250] $\mu\text{m}$ (mJy)	[350] $\mu\text{m}$ (mJy)	[500] $\mu\text{m}$ (mJy)					
(1)	(2)	(3)	(4)	(5)	(6)	(7)	(8)	(9)	(10)	(11)	(12)	(13)	(14)	(15)					
15	IRAS 05184+3635	109 $\pm$ 11	266 $\pm$ 53			440 $\pm$ 57	523 $\pm$ 68	5800 $\pm$ 638	19500 $\pm$ 5070	391 $\pm$ 64	6942 $\pm$ 5.215**								
31										1415 $\pm$ 10.552*									
51										928 $\pm$ 152									
60																			
85										1006 $\pm$ 103									
90	IRAS 05177+3636	224 $\pm$ 22				738 $\pm$ 52	1590 $\pm$ 127	4290 $\pm$ 987	15900 $\pm$ 2703	130 $\pm$ 41	1059 $\pm$ 94	4069 $\pm$ 671							
92										2322 $\pm$ 20									
95																			
96										1006 $\pm$ 103									
97																			
101	G170.7247-00.1388	171 $\pm$ 20								814 $\pm$ 125		1444 $\pm$ 979							
112	G170.7196-00.1118	181 $\pm$ 21								2951 $\pm$ 34		7689 $\pm$ 279							
126										2951 $\pm$ 34		7689 $\pm$ 279							
128										1261 $\pm$ 58		3683 $\pm$ 349							
130										2693 $\pm$ 70		5185 $\pm$ 594							
177										5163 $\pm$ 813									
178	G170.6589-00.2334	159 $\pm$ 19		859 $\pm$ 143								291 $\pm$ 47							
182	G170.6758-00.2691	185 $\pm$ 22	662 $\pm$ 132	525 $\pm$ 105	2450 $\pm$ 408	1160 $\pm$ 81	6340 $\pm$ 444	167000 $\pm$ 23380	379000 $\pm$ 45480	1735 $\pm$ 75		5052 $\pm$ 7.704**							
183	IRAS 05168+3634	891 $\pm$ 89	1450 $\pm$ 171	1370 $\pm$ 161						4472 $\pm$ 103		11125 $\pm$ 1724							
189	IRAS 05162+3639									109 $\pm$ 32									
190										1545 $\pm$ 12		2814 $\pm$ 74							
192										1545 $\pm$ 12		2814 $\pm$ 74							
216												7684 $\pm$ 212	4171.5 $\pm$ 111	2295 $\pm$ 72					
219	IRAS 05156+3643	455 $\pm$ 46	797 $\pm$ 159			649 $\pm$ 58	947 $\pm$ 85	1810 $\pm$ 181	3020 $\pm$ 332			7684 $\pm$ 212	4171.5 $\pm$ 111	2295 $\pm$ 72					
229										270 $\pm$ 22		7684 $\pm$ 212	4171.5 $\pm$ 111	2295 $\pm$ 72					
232																			
234										185 $\pm$ 12		1128 $\pm$ 66	2031 $\pm$ 119						
238										853 $\pm$ 18									
239	240									892 $\pm$ 29		2668 $\pm$ 136	6201 $\pm$ 102	7098.4 $\pm$ 126					
240										144 $\pm$ 43		932 $\pm$ 149		5575 $\pm$ 105					

**Notes.** (1) - ID number of sub-regions members taken from Table 5, (2)- Names of IRAS and MSX sources, (3)-(6)- measured fluxes with errors in MSX catalog, (7)-10)-measured fluxes with errors in IRAS catalog, (11)-(12)- measured fluxes with errors in *Herschel* PACS 70 and 160  $\mu\text{m}$  catalogs, (13)-(15)-measured fluxes with errors in *Herschel* SPIRE 250, 350 and 500  $\mu\text{m}$  catalogs, <sup>(\*)</sup> -fluxes taken from *Herschel* PACS: Extended source list catalog in blue band (70  $\mu\text{m}$ ), <sup>(\*\*)</sup> - fluxes taken from *Herschel* PACS: Extended source list catalog in red band (160  $\mu\text{m}$ )

**Table 7.** Parameters derived from [Robitaille et al. \(2007\)](#) models SED fitting for two distances.

ID	$A_v$		Stellar age		Stellar mass		Temperature		MdotE		MdotD		$L_{Total}$		$N_{fit}$		$N_{data}$
	(mag)		(Log)(yr)		( $M_\odot$ )		(Log)(K)		(Log)( $M_\odot yr^{-1}$ )		(Log)( $M_\odot yr^{-1}$ )		(Log)( $L_\odot$ )				
	1.88	6.1	1.88	6.1	1.88	6.1	1.88	6.1	1.88	6.1	1.88	6.1	1.88	6.1	1.88	6.1	
(1)	(2)	(3)	(4)	(5)	(6)	(7)	(8)	(9)	(10)	(11)	(12)	(13)	(14)	(15)	(16)	(17)	(18)
IRAS 05184+3635																	
31	12.1 ± 2.0	6.9 ± 0.3	6.6 ± 5.9	5.9 ± 5.8	3.1 ± 0.6	6.8 ± 0.7	4.1 ± 3.3	4.1 ± 3.9	0.0 ± 0.0	-5.3 ± -5.2	-8.4 ± -8.4	-7.6 ± -7.5	1.9 ± 1.5	3.0 ± 2.8	29	2	8
46	12.9 ± 3.0	13.0 ± 3.8	6.5 ± 6.5	6.2 ± 6.0	2.2 ± 0.4	4.4 ± 0.8	3.9 ± 3.2	4.0 ± 3.3	-4.9 ± -4.6	-4.4 ± -4.1	-6.9 ± -6.8	-6.2 ± -5.8	1.7 ± 1.8	2.4 ± 1.7	71	76	9
47	13.1 ± 2.9	13.1 ± 3.9	6.7 ± 6.3	6.2 ± 6.0	2.2 ± 0.4	4.4 ± 0.8	3.9 ± 3.3	4.0 ± 3.3	-4.9 ± -4.6	-4.4 ± -4.1	-6.8 ± -6.8	-6.2 ± -5.8	1.7 ± 1.7	2.4 ± 1.7	70	71	9
48	11.7 ± 1.2	11.5 ± 2.1	6.6 ± 6.3	5.9 ± 5.8	0.6 ± 0.2	1.4 ± 0.7	3.6 ± 2.5	3.6 ± 2.6	-5.9 ± -5.0	-5.4 ± -4.8	-7.8 ± -6.4	-7.6 ± -7.0	0.0 ± 0.4	0.9 ± 1.1	3859	2238	7
51	21.1 ± 3.3	15.7 ± 2.7	5.8 ± 5.6	6.0 ± 5.2	3.7 ± 0.7	4.8 ± 0.8	3.8 ± 3.1	4.1 ± 3.4	-5.5 ± -5.5	-5.9 ± -5.8	-7.1 ± -6.9	-6.5 ± -6.3	1.9 ± 1.6	2.7 ± 2.1	57	46	10
52	12.0 ± 2.4	16.4 ± 5.1	5.2 ± 5.1	5.7 ± 5.7	0.8 ± 0.3	4.3 ± 1.1	3.6 ± 2.7	3.8 ± 3.2	-5.3 ± -5.3	-4.8 ± -4.9	-6.2 ± -6.4	-6.1 ± -6.0	0.9 ± 0.5	2.2 ± 1.8	115	54	9
26	5.6 ± 1.3	3.5 ± 2.1	5.9 ± 6.2	5.9 ± 5.9	0.4 ± 0.4	1.4 ± 1.1	3.5 ± 3.0	3.7 ± 3.4	-4.8 ± -5.1	-4.5 ± -4.2	-7.4 ± -7.2	-6.0 ± -5.9	0.2 ± 0.1	1.8 ± 2.0	17	30	9
34	10.5 ± 2.7	9.6 ± 1.9	6.6 ± 6.4	6.7 ± 6.2	1.5 ± 0.5	2.8 ± 0.5	3.7 ± 3.2	4.0 ± 3.3	-6.3 ± -5.9	-7.1 ± -6.3	-7.5 ± -7.4	-8.0 ± -7.6	0.9 ± 0.8	1.8 ± 1.3	68	216	9
42	11.7 ± 1.5	6.8 ± 1.5	6.5 ± 6.2	6.6 ± 6.2	2.6 ± 0.4	3.8 ± 0.7	3.8 ± 3.2	4.1 ± 3.4	-6.3 ± -6.1	-5.9 ± -5.6	-7.4 ± -7.4	-7.1 ± -7.0	1.5 ± 1.0	2.2 ± 1.5	439	193	9
1	0.0 ± 0.0	0.0 ± 0.0	6.1 ± 4.9	6.5 ± 5.8	3.4 ± 0.1	6.9 ± 0.1	3.8 ± 2.3	4.3 ± 2.6	0.0 ± 0.0	0.0 ± 0.0	-12.6 ± -12.5	-11.7 ± -12.1	1.7 ± 0.2	3.2 ± 1.5	11	3	9
32	10.2 ± 1.9	5.5 ± 1.4	6.8 ± 6.1	5.7 ± 5.6	2.3 ± 0.5	2.6 ± 0.5	4.0 ± 3.2	3.7 ± 2.9	-5.5 ± -5.3	-4.4 ± -4.5	-8.2 ± -8.0	-6.6 ± -6.9	1.5 ± 0.9	1.7 ± 1.4	59	83	9
39	5.9 ± 0.5	6.1 ± 1.4	5.5 ± 4.5	5.3 ± 4.7	0.9 ± 0.1	3.3 ± 0.6	3.6 ± 2.4	3.7 ± 2.9	-5.3 ± -5.8	-4.4 ± -4.6	-7.6 ± -7.8	-7.1 ± -7.1	0.7 ± -0.3	1.8 ± 1.1	465	124	9
41	5.9 ± 0.5	6.2 ± 1.5	5.5 ± 4.5	5.3 ± 4.7	0.9 ± 0.1	3.3 ± 0.7	3.6 ± 2.4	3.7 ± 2.9	-5.3 ± -5.8	-4.4 ± -4.6	-7.6 ± -7.8	-7.1 ± -7.1	0.7 ± -0.3	1.8 ± 1.1	473	125	9
17	5.3 ± 0.3	2.9 ± 0.5	6.3 ± 5.6	6.4 ± 5.3	1.7 ± 0.1	3.5 ± 0.3	3.7 ± 2.6	3.9 ± 2.7	-6.7 ± -6.7	-5.8 ± -6.0	-7.7 ± -8.0	-7.4 ± -7.9	0.8 ± -0.2	1.9 ± 0.8	905	254	9
29	3.4 ± 1.2	4.6 ± 0.8	5.5 ± 5.7	5.4 ± 4.7	0.5 ± 0.4	1.9 ± 0.3	3.6 ± 2.9	3.6 ± 2.6	-4.9 ± -5.0	-4.5 ± -4.5	-7.7 ± -7.5	-7.0 ± -7.0	0.6 ± 0.7	1.2 ± 0.6	69	133	9
16	4.7 ± 2.2	6.0 ± 2.1	6.5 ± 6.3	6.7 ± 6.3	0.6 ± 0.1	1.9 ± 0.6	3.6 ± 2.5	3.9 ± 3.4	-5.7 ± -5.4	-6.0 ± -5.8	-7.2 ± -7.4	-7.1 ± -7.3	0.2 ± 0.0	1.3 ± 0.9	12	35	9
22	4.9 ± 0.8	4.9 ± 0.8	6.3 ± 6.0	6.3 ± 6.0	0.3 ± 0.1	1.3 ± 0.3	3.5 ± 2.7	3.7 ± 2.9	-6.7 ± -6.7	-5.7 ± -5.4	-8.3 ± -8.5	-7.3 ± -7.4	-0.5 ± -1.1	0.8 ± 0.5	602	511	8
45	7.4 ± 2.5	10.3 ± 2.8	6.2 ± 6.1	6.1 ± 6.1	0.6 ± 0.2	1.5 ± 0.7	3.6 ± 2.9	3.8 ± 3.3	-4.5 ± -4.4	-5.1 ± -5.0	-6.3 ± -5.7	-7.5 ± -7.3	0.7 ± 0.8	1.5 ± 1.5	98	617	8
15	2.7 ± 0.3	2.7 ± 0.3	5.9 ± 5.2	5.3 ± 4.7	1.1 ± 0.2	2.3 ± 0.5	3.7 ± 2.7	3.7 ± 2.8	-4.8 ± -5.7	-4.0 ± -4.5	-6.7 ± -7.2	-6.9 ± -7.3	1.3 ± 0.5	1.7 ± 1.2	73	121	6
24	0.6 ± 0.0	6.6 ± 4.4	6.3 ± 0.0	6.3 ± 6.2	1.4 ± 0.0	1.6 ± 1.0	3.7 ± 0.0	3.8 ± 3.5	0.0 ± 0.0	-4.9 ± -4.5	-7.4 ± 0.0	-7.1 ± -6.7	0.4 ± 0.0	1.6 ± 1.7	1	60	9
25	1.1 ± 0.0	6.3 ± 4.4	6.3 ± 0.0	6.2 ± 6.2	1.4 ± 0.0	1.5 ± 0.9	3.7 ± 0.0	3.7 ± 3.4	0.0 ± 0.0	-4.8 ± -4.5	-7.4 ± 0.0	-7.1 ± -6.7	0.4 ± 0.0	1.4 ± 1.6	1	46	9
IRAS 05177+3636																	
97	4.4 ± 1.8	3.0 ± 1.0	5.8 ± 5.9	4.1 ± 4.0	2.6 ± 1.3	5.5 ± 0.9	3.8 ± 3.6	3.6 ± 2.8	-4.1 ± -3.9	-3.5 ± -3.6	-6.0 ± -5.8	-5.0 ± -5.0	2.4 ± 2.5	2.6 ± 2.0	122	51	8
101	8.6 ± 1.9	2.0 ± 1.0	6.3 ± 6.1	6.0 ± 5.3	4.2 ± 0.8	5.5 ± 0.6	3.9 ± 3.3	4.2 ± 3.3	-6.2 ± -6.4	-7.3 ± -7.4	-7.7 ± -7.5	-7.1 ± -6.7	2.2 ± 1.6	2.9 ± 2.1	58	38	12
128	19.5 ± 3.3	8.1 ± 0.8	5.9 ± 5.1	6.0 ± 4.8	4.5 ± 0.7	5.5 ± 0.3	3.9 ± 2.8	4.2 ± 3.0	-7.0 ± -7.1	-8.3 ± -9.6	-7.5 ± -7.6	-6.4 ± -7.7	2.4 ± 1.7	2.8 ± 1.6	3	8	12
126	10.3 ± 4.8	10.2 ± 5.0	5.0 ± 4.6	4.9 ± 4.6	2.1 ± 0.6	6.8 ± 0.7	3.6 ± 2.6	3.7 ± 2.8	-3.7 ± -3.9	-3.4 ± -3.8	-6.3 ± -6.3	-6.0 ± -5.8	1.6 ± 1.1	2.6 ± 1.8	17	12	11
123	5.7 ± 2.1	9.0 ± 2.7	5.1 ± 5.1	6.3 ± 6.2	0.4 ± 0.2	1.0 ± 0.6	3.6 ± 2.6	3.7 ± 3.3	-4.6 ± -4.2	-5.0 ± -4.8	-7.5 ± -7.3	-7.0 ± -6.9	0.5 ± 0.5	1.3 ± 1.2	88	108	8
125	6.2 ± 1.2	9.4 ± 1.9	4.8 ± 4.6	5.3 ± 4.9	0.3 ± 0.1	2.2 ± 0.5	3.5 ± 2.6	3.7 ± 2.8	-5.0 ± -4.9	-4.8 ± -4.9	-7.2 ± -7.7	-6.7 ± -7.0	0.3 ± -0.2	1.5 ± 1.0	191	166	7
130	29.0 ± 6.1	28.9 ± 6.3	4.8 ± 5.0	4.8 ± 4.9	1.6 ± 0.6	4.6 ± 1.9	3.6 ± 2.7	3.7 ± 3.1	-4.2 ± -4.6	-3.6 ± -4.0	-6.2 ± -6.0	-5.0 ± -5.0	1.6 ± 1.4	2.5 ± 2.0	39	7	9
129	31.9 ± 4.5	27.7 ± 3.7	6.6 ± 6.1	6.5 ± 5.9	3.5 ± 0.5	5.7 ± 0.7	4.1 ± 3.3	4.3 ± 3.4	-6.1 ± -5.4	-5.1 ± -4.5	-7.5 ± -7.2	-5.9 ± -5.3	2.1 ± 1.4	3.0 ± 2.4	442	252	8
92	0.7 ± 0.5	0.5 ± 0.6	5.1 ± 4.6	4.7 ± 4.4	2.3 ± 0.6	4.3 ± 1.1	3.6 ± 2.8	3.7 ± 3.1	-4.2 ± -4.2	-3.2 ± -3.6	-7.7 ± -7.5	-6.6 ± -6.6	1.6 ± 1.1	2.2 ± 1.4	6	2	11
85	9.3 ± 2.7	3.8 ± 1.7	5.9 ± 5.5	5.8 ± 5.4	3.7 ± 0.7	5.2 ± 0.6	3.8 ± 3.0	4.0 ± 3.4	-4.8 ± -4.5	-4.6 ± -3.9	-7.0 ± -7.4	-6.7 ± -6.2	2.0 ± 1.5	2.6 ± 1.8	22	45	7
112	6.4 ± 2.1	5.6 ± 1.2	3.6 ± 3.6	3.8 ± 3.5	0.8 ± 0.2	4.1 ± 1.8	3.6 ± 3.0	3.6 ± 3.2	-3.5 ± -4.1	-2.8 ± -3.2	-6.2 ± -6.1	-5.2 ± -5.4	1.3 ± 0.7	2.4 ± 2.0	7	3	7
131	12.3 ± 3.0	9.2 ± 3.7	5.5 ± 5.3	4.9 ± 4.7	1.2 ± 0.5	3.8 ± 1.4	3.7 ± 2.9	3.7 ± 3.0	-5.0 ± -5.2	-4.1 ± -4.2	-7.4 ± -7.3	-6.8 ± -6.9	1.2 ± 1.1	2.1 ± 1.6	117	10	8
96	0.6 ± 0.5	0.2 ± 0.3	3.2 ± 2.3	3.5 ± 3.5	0.3 ± 0.2	2.3 ± 0.2	3.5 ± 2.5	3.6 ± 2.2	-5.3 ± -5.4	-4.6 ± -5.7	-4.9 ± -5.2	-4.6 ± -4.8	1.2 ± 0.5	2.3 ± 1.6	3	3	9
103	4.1 ± 1.2	5.5 ± 1.8	5.5 ± 5.0	5.5 ± 5.4	1.2 ± 0.4	3.3 ± 0.7	3.6 ± 2.8	3.7 ± 3.0	-4.8 ± -4.9	-4.4 ± -4.3	-7.6 ± -7.6	-6.6 ± -6.4	0.9 ± 0.6	1.8 ± 1.5	33	163	9
93	4.7 ± 1.4	1.8 ± 0.9	6.1 ± 6.1	5.6 ± 5.7	1.6 ± 0.6	2.3 ± 0.6	3.7 ± 3.2	3.7 ± 3.1	-5.1 ± -4.9	-4.4 ± -4.4	-8.3 ± -7.8	-7.1 ± -7.0	1.2 ± 1.2	1.6 ± 1.4	125	186	9
60	0.7 ± 1.2	1.1 ± 1.0	4.6 ± 3.3	4.9 ± 4.2	0.4 ± 0.1	2.3 ± 0.4	3.6 ± 2.3	3.6 ± 2.5	-4.0 ± -4.7	-3.4 ± -4.1	-9.0 ± -9.2	-6.8 ± -7.8	0.5 ± 0.0	1.7 ± 1.2	3	4	8
95	2.5 ± 1.6	1.8 ± 0.7	4.9 ± 4.8	5.0 ± 4.8	0.3 ± 0.1	1.2 ± 0.6	3.5 ± 2.8	3.6 ± 2.8	-4.9 ± -5.0	-4.5 ± -4.6	-7.3 ± -7.4	-6.9 ± -7.1	0.2 ± -0.1	1.1 ± 0.8	34	20	10
110	8.6 ± 3.3	5.6 ± 1.6	6.4 ± 6.3	5.7 ± 5.9	1.4 ± 0.9	1.9 ± 0.7	3.8 ± 3.5	3.7 ± 3.2	-5.5 ± -5.4	-4.8 ± -4.7	-8.3 ± -7.8	-7.4 ± -7.1	1.4 ± 1.4	1.4 ± 1.5	102	283	9
102	8.5 ± 2.1	8.8 ± 1.9	6.5 ± 6.3	6.2 ± 6.0	0.8 ± 0.4	2.2 ± 0.6	3.6 ± 2.9	3.8 ± 3.3	-7.1 ± -6.8	-5.7 ± -5.6	-8.2 ± -8.2	-7.3 ± -7.4	-0.1 ± -0.3	1.6 ± 1.6	47	108	8
82	3.7 ± 0.3	3.1 ± 0.5	6.4 ± 5.7	6.1 ± 5.7	1.4 ± 0.1	3.5 ± 0.6	3.7 ± 2.7	3.8 ± 2.9	-6.7 ± -6.8	-6.4 ± -6.8	-7.7 ± -8.0	-7.1 ± -7.6	0.5 ± -0.4	1.5 ± 0.7	405	138	9
91	4.2 ± 0.5	4.2 ± 1.0	6.1 ± 5.6	5.7 ± 5.2	0.9 ± 0.2	3.1 ± 0.6	3.6 ± 2.6	3.7 ± 2.9	-6.0 ± -6.1	-5.4 ± -5.2	-8.0 ± -8.1	-7.4 ± -7.4	0.4 ± -0.1	1.5 ± 0.8	911	163	9
88	3.5 ± 0.3	3.6 ± 0.2	6.1 ± 5.4	5.8 ± 4.6	0.9 ± 0.1	3.2 ± 0.2	3.6 ± 2.5	3.7 ± 2.6	-5.9 ± -6.3	-5.4 ± -5.9	-7.8 ± -8.2	-7.2 ± -7.8	0.4 ± -0.4	1.5 ± 0.3	754	155	9
104	4.4 ± 1.4	5.8 ± 1.1	5.0 ± 4.7	5.7 ± 5.4	0.2 ± 0.1	1.4 ± 0.3	3.5 ± 2.8	3.7 ± 2.9	-5.0 ± -5.2	-4.7 ± -4.9	-8.0 ± -8.0	-6.9 ± -7.1	0.0 ± -0.1	1.5 ± 1.2	53	152	9
89	4.4 ± 0.2	5.3 ± 0.5	6.2 ± 5.0	6.5 ± 5.8	0.6 ± 0.1	2.5 ± 0.3	3.6 ± 2.3	3.8 ± 2.9	-6.1 ± -7.1	-6.4 ± -6.6	-7.9 ± -8.7	-7.4 ± -7.5	0.2 ± -0.6	1.3 ± 0.3			

172	9.9 ± 1.4	10.0 ± 1.5	6.7 ± 6.3	5.9 ± 5.7	0.7 ± 0.2	1.3 ± 0.6	3.6 ± 2.4	3.6 ± 2.5	-5.5 ± -4.8	-5.5 ± -4.9	-7.7 ± -7.0	-7.7 ± -7.1	0.2 ± 0.5	0.8 ± 1.1	1384	2004	7
174	11.6 ± 2.5	3.3 ± 1.7	6.2 ± 5.8	5.3 ± 4.9	2.6 ± 0.6	2.7 ± 0.8	3.7 ± 3.0	3.7 ± 2.4	-6.8 ± -6.3	-5.3 ± -5.7	-9.9 ± -9.4	-7.4 ± -7.2	1.1 ± 0.5	1.5 ± 0.8	142	9	8
185	17.1 ± 2.0	16.4 ± 3.6	5.9 ± 5.6	5.3 ± 5.0	1.1 ± 0.3	3.0 ± 0.9	3.6 ± 2.6	3.7 ± 2.9	-5.5 ± -5.0	-4.3 ± -4.1	-7.8 ± -7.5	-6.8 ± -6.3	0.6 ± 0.5	1.7 ± 1.5	3544	424	7
187	14.4 ± 3.1	13.3 ± 3.4	5.0 ± 4.8	4.8 ± 4.6	1.5 ± 0.5	4.6 ± 1.2	3.6 ± 2.8	3.7 ± 2.8	-4.2 ± -4.3	-3.8 ± -3.9	-6.5 ± -6.2	-6.0 ± -5.7	1.4 ± 1.0	2.3 ± 1.9	175	102	8
162	4.9 ± 1.8	4.7 ± 0.7	5.6 ± 5.5	5.7 ± 5.1	2.7 ± 0.8	5.5 ± 0.6	3.7 ± 3.1	4.0 ± 3.0	-4.3 ± -4.4	-4.1 ± -4.4	-6.1 ± -5.8	-5.4 ± -5.4	1.9 ± 1.5	2.7 ± 1.7	47	47	9
188	23.9 ± 6.4	23.3 ± 5.8	5.4 ± 5.5	5.2 ± 5.0	0.9 ± 0.5	3.4 ± 1.0	3.6 ± 2.9	3.7 ± 2.5	-5.0 ± -4.7	-4.3 ± -4.1	-7.4 ± -7.0	-6.7 ± -6.5	0.9 ± 1.0	1.8 ± 1.3	854	422	8
159	2.1 ± 0.8	3.6 ± 0.9	5.4 ± 4.9	5.3 ± 4.6	1.2 ± 0.3	3.5 ± 0.5	3.6 ± 2.8	3.7 ± 2.7	-5.0 ± -5.4	-4.3 ± -4.5	-7.5 ± -7.4	-6.8 ± -6.8	1.0 ± 0.5	1.8 ± 1.1	76	119	9
143	1.3 ± 0.2	2.1 ± 0.5	5.9 ± 5.1	5.8 ± 5.5	2.7 ± 0.5	5.3 ± 1.1	3.8 ± 3.0	4.1 ± 3.6	-4.4 ± -5.0	-3.5 ± -3.6	-6.8 ± -7.1	-6.0 ± -5.9	1.9 ± 1.0	2.7 ± 2.3	19	27	7
132	0.0 ± 0.0	0.0 ± 0.0	5.3 ± 5.1	5.0 ± 3.4	1.9 ± 0.4	5.0 ± 0.1	3.7 ± 2.1	3.7 ± 2.1	-4.9 ± -4.7	-3.4 ± -4.9	-7.6 ± -7.5	-7.5 ± -9.1	1.3 ± 0.4	2.2 ± 0.6	9	2	9
164	9.2 ± 2.1	9.0 ± 2.4	5.6 ± 5.5	5.7 ± 5.6	1.2 ± 0.5	4.1 ± 0.9	3.6 ± 2.8	3.8 ± 3.2	-5.4 ± -5.2	-4.6 ± -4.4	-7.5 ± -7.4	-7.3 ± -7.2	0.9 ± 0.7	2.0 ± 1.5	761	164	9
160	10.8 ± 1.6	8.3 ± 1.7	6.6 ± 6.3	6.6 ± 6.2	1.5 ± 0.4	3.1 ± 0.4	3.7 ± 3.1	4.0 ± 3.3	-6.8 ± -6.3	-7.9 ± -7.1	-8.1 ± -7.8	-8.1 ± -7.5	0.8 ± 0.7	1.9 ± 1.4	126	189	8
149	6.0 ± 2.0	6.1 ± 1.6	6.6 ± 6.5	6.1 ± 5.5	0.9 ± 0.4	2.7 ± 0.7	3.6 ± 3.0	3.7 ± 3.1	-6.6 ± -6.4	-6.3 ± -6.2	-8.3 ± -8.2	-7.7 ± -7.5	0.1 ± -0.2	1.5 ± 1.6	73	49	8
146	2.9 ± 0.3	3.1 ± 0.4	6.1 ± 5.6	6.5 ± 5.9	0.6 ± 0.1	2.7 ± 0.3	3.6 ± 2.6	3.8 ± 2.9	-6.2 ± -6.4	-6.6 ± -6.6	-7.8 ± -8.2	-7.3 ± -7.4	0.1 ± -0.5	1.4 ± 0.5	443	315	8
140	1.7 ± 0.2	2.0 ± 0.4	6.2 ± 5.4	6.1 ± 5.7	0.6 ± 0.1	2.5 ± 0.4	3.6 ± 2.5	3.7 ± 2.8	-6.4 ± -6.5	-6.1 ± -6.2	-8.5 ± -8.8	-7.8 ± -7.7	0.0 ± -0.9	1.2 ± 0.4	2350	613	8
170	5.7 ± 1.8	8.8 ± 1.8	5.9 ± 5.9	6.2 ± 5.9	0.6 ± 0.2	1.4 ± 0.5	3.6 ± 2.7	3.8 ± 3.1	-4.3 ± -4.2	-5.1 ± -5.1	-5.8 ± -5.4	-7.1 ± -7.1	1.0 ± 1.2	1.4 ± 1.3	79	255	8
137	2.6 ± 0.9	5.4 ± 1.0	6.1 ± 5.8	6.5 ± 6.0	0.3 ± 0.1	2.0 ± 0.4	3.5 ± 2.7	3.9 ± 3.1	-5.5 ± -5.6	-4.5 ± -4.3	-7.6 ± -7.9	-7.0 ± -6.5	0.0 ± -0.4	1.7 ± 1.3	57	184	8
IRAS 05162+3639																	
190	6.3 ± 3.1	7.8 ± 2.5	4.8 ± 4.7	4.2 ± 4.0	1.0 ± 0.4	3.1 ± 0.6	3.6 ± 2.7	3.6 ± 2.8	-3.9 ± -4.2	-3.3 ± -3.7	-6.3 ± -6.1	-5.7 ± -5.6	1.2 ± 0.5	2.1 ± 1.4	37	21	8
192	34.6 ± 3.0	19.5 ± 3.8	5.9 ± 5.2	6.0 ± 5.2	4.5 ± 0.3	5.4 ± 0.2	3.9 ± 3.0	4.2 ± 3.0	-5.6 ± -5.5	-7.2 ± -7.2	-7.5 ± -7.7	-6.7 ± -6.8	2.2 ± 1.8	2.8 ± 1.7	20	15	12
189	7.7 ± 2.5	8.3 ± 2.2	5.0 ± 4.7	5.3 ± 4.9	0.2 ± 0.1	1.1 ± 0.3	3.5 ± 2.6	3.6 ± 2.8	-5.2 ± -5.1	-4.8 ± -4.7	-7.5 ± -7.7	-7.2 ± -7.0	-0.1 ± -0.3	0.9 ± 0.4	31	39	10
191	17.8 ± 1.8	18.1 ± 1.8	6.1 ± 5.6	6.2 ± 5.7	0.6 ± 0.1	2.1 ± 0.3	3.6 ± 2.6	3.8 ± 2.9	-5.8 ± -6.1	-5.2 ± -5.2	-7.8 ± -8.3	-6.6 ± -6.3	0.0 ± -0.4	1.6 ± 1.6	160	178	8
193	12.6 ± 2.4	10.8 ± 1.6	6.4 ± 6.0	5.7 ± 5.5	0.5 ± 0.2	0.9 ± 0.2	3.6 ± 2.7	3.6 ± 2.7	-6.3 ± -5.9	-5.3 ± -5.5	-7.9 ± -8.1	-7.5 ± -7.7	-0.1 ± -0.4	0.9 ± 0.7	88	310	8
IRAS 05156+3643																	
234	2.1 ± 0.8	1.4 ± 1.9	6.2 ± 6.3	3.8 ± 2.7	3.4 ± 3.6	2.9 ± 1.2	4.1 ± 3.9	3.6 ± 2.5	-6.0 ± -5.9	-4.7 ± -5.4	-4.8 ± -5.1	-4.6 ± -4.7	3.2 ± 3.4	2.3 ± 0.4	4	2	14
239	22.8 ± 1.5	14.0 ± 1.0	5.6 ± 4.5	6.0 ± 5.5	4.4 ± 0.3	4.7 ± 0.5	3.7 ± 2.6	4.1 ± 3.5	-5.1 ± -6.2	-5.6 ± -5.2	-8.9 ± -10.0	-6.1 ± -5.7	2.0 ± 0.9	2.6 ± 1.7	7	17	11
240	21.1 ± 2.1	20.5 ± 3.0	4.9 ± 4.5	4.9 ± 4.6	0.4 ± 0.1	1.6 ± 0.3	3.6 ± 2.6	3.6 ± 2.6	-4.2 ± -4.6	-3.5 ± -4.0	-8.0 ± -7.9	-7.8 ± -7.5	0.3 ± -0.3	1.4 ± 0.7	11	6	10
232	4.6 ± 2.5	4.4 ± 2.4	3.6 ± 3.3	4.3 ± 4.3	0.2 ± 0.0	1.3 ± 0.3	3.5 ± 2.5	3.6 ± 2.6	-5.7 ± -6.1	-5.0 ± -5.4	-6.3 ± -6.5	-5.9 ± -5.9	0.4 ± -0.5	1.5 ± 0.7	51	63	10
218	3.6 ± 1.7	8.1 ± 2.1	6.0 ± 6.2	6.7 ± 6.2	0.8 ± 0.6	2.1 ± 0.4	3.6 ± 3.0	3.9 ± 3.2	-4.9 ± -5.0	-4.6 ± -4.6	-7.4 ± -7.2	-6.6 ± -6.3	0.7 ± 0.6	1.5 ± 0.8	23	69	9
219	9.7 ± 2.9	5.4 ± 2.8	6.5 ± 6.5	5.5 ± 5.3	3.2 ± 0.5	5.2 ± 1.0	3.9 ± 3.4	3.8 ± 3.1	-8.3 ± -8.1	-5.4 ± -5.3	-7.3 ± -7.4	-6.0 ± -5.6	1.8 ± 1.4	2.4 ± 1.8	5	18	11
236	4.8 ± 1.2	4.5 ± 1.0	5.0 ± 5.0	5.3 ± 5.4	0.6 ± 0.2	1.9 ± 0.6	3.6 ± 2.7	3.6 ± 2.8	-4.3 ± -4.7	-3.9 ± -4.3	-6.2 ± -6.1	-5.8 ± -5.6	1.0 ± 0.7	1.9 ± 1.6	298	385	8
225	3.8 ± 0.9	4.4 ± 1.0	4.8 ± 4.3	5.4 ± 5.2	0.3 ± 0.1	1.9 ± 0.3	3.5 ± 2.8	3.7 ± 2.8	-4.6 ± -5.0	-4.4 ± -4.5	-7.3 ± -7.6	-6.5 ± -6.8	0.3 ± -0.2	1.4 ± 0.9	61	167	9
227	6.3 ± 0.3	0.0 ± 0.0	6.1 ± 4.7	6.2 ± 4.2	3.4 ± 0.1	6.1 ± 0.1	3.7 ± 2.4	4.3 ± 2.3	0.0 ± 0.0	0.0 ± 0.0	-11.9 ± -13.3	-11.5 ± -13.5	1.6 ± 0.2	3.0 ± 1.0	6	3	8
228	6.9 ± 1.0	7.0 ± 1.0	6.2 ± 5.8	6.4 ± 5.9	0.4 ± 0.1	2.1 ± 0.3	3.5 ± 2.7	3.8 ± 2.9	-6.0 ± -6.1	-6.0 ± -5.8	-7.9 ± -8.2	-7.2 ± -7.2	-0.1 ± -0.8	1.3 ± 0.7	605	559	8
204	1.0 ± 0.9	3.5 ± 2.2	5.0 ± 4.9	6.6 ± 6.5	0.7 ± 0.5	2.1 ± 0.9	3.6 ± 2.7	3.9 ± 3.4	-3.9 ± -3.8	-4.1 ± -3.6	-7.0 ± -6.9	-7.5 ± -7.1	1.0 ± 1.0	1.6 ± 1.6	34	63	8
213	–	5.7 ± 0.9	–	6.6 ± 6.1	–	1.9 ± 0.4	–	3.8 ± 3.2	–	-6.9 ± -6.7	–	-7.6 ± -7.8	–	1.2 ± 1.0	–	651	7

**Notes.** (1)-ID number of sub-regions members taken from Table 5, (2)-(15)-are the weighted means and the standard deviations of parameters obtained by fitting tool for all models with best  $\chi^2 - \chi^2_{best} < 3N$  at two distances: 1.88 and 6.1 kpc, (16),(17)-are number of fitting models at two distances: 1.88 and 6.1 kpc, (18)-is the number of input fluxes.